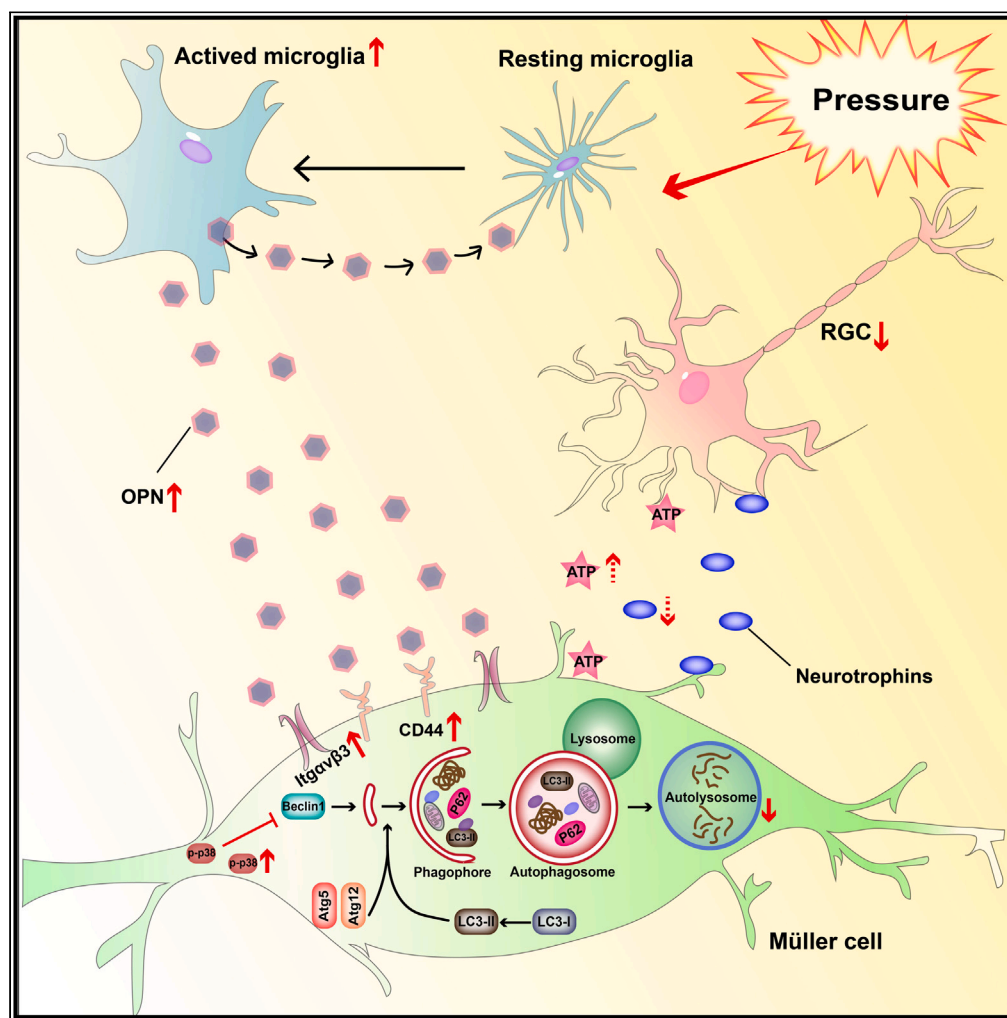


Article

Molecular signaling from microglia impacts macroglia autophagy and neurons survival in glaucoma



Huan Yu, Huimin Zhong, Jun Sun, ..., Xi Shen, Shouyue Huang, Yisheng Zhong

pinghpingh@126.com (P.H.)
carl_shen2005@126.com (X.S.)
yachtjj@hotmail.com (S.H.)
yszong68@126.com (Y.Z.)

Highlights

In the context of glaucoma, microglia-derived OPN down-regulates Müller autophagy

Altered levels of Müller autophagy ultimately increase RGCs loss

P38-MAKP pathway significantly regulates the crosstalk between macroglia and microglia

Yu et al., iScience 26, 106839
June 16, 2023 © 2023 The Author(s).
<https://doi.org/10.1016/j.isci.2023.106839>



Article

Molecular signaling from microglia impacts macroglia autophagy and neurons survival in glaucoma

Huan Yu,^{1,5} Huimin Zhong,^{2,5} Jun Sun,¹ Na Li,¹ Junjue Chen,¹ Bingqiao Shen,¹ Ping Huang,^{3,*} Xi Shen,^{1,*} Shouyue Huang,^{1,*} and Yisheng Zhong^{1,4,6,*}

SUMMARY

Interactions between microglia and macroglia play important roles in the neurodegeneration of the central nervous system and so is the situation between microglia and Müller cells in retina neurodegenerations like glaucoma. This study focuses on the roles of microglia-derived osteopontin (OPN) in impacting Müller cells and retinal ganglion cells (RGCs). Rat model and cell pressurization culture were used to simulate glaucoma scenarios. Animals were differently treated with anti-OPN, suppressors of OPN receptors (Itg α v β 3/CD44) or microglia inhibitor minocycline, while isolated retinal Müller cells were accordingly treated with conditioned media from microglia culture pretreated with pressuring, overexpression-OPN, SiR-OPN, or minocycline. SB203580 was introduced to explore the role of p38 MAPK signaling pathway. Results revealed microglia may secrete OPN to impact Müller cells' autophagy and RGCs survival via binding to Itg α v β 3/CD44 receptors in glaucomatous neurodegeneration with involvement of p38 MAPK pathway. This discovery may benefit understanding neurodegenerative disorders and exploring therapeutics.

INTRODUCTION

It is acknowledged that microglia and macroglia exert pivotal impacts on neurons in the central nervous system (CNS) under both healthy and disease conditions.^{1–3} Research focusing on the interaction between microglia and macroglia in the context of neurodegeneration has found that this signaling communication plays a critical role in regulating the overall pathophysiological process, where the dynamic alterations directly influence the glia response, yielding either protective or detrimental results toward neurons.^{4–6} The interaction is reciprocal, establishing crosstalk between glia and neurons. This provides a promising target for neuromodulation in treating neurodegenerative disorders.

Glaucoma describes a group of diseases that are characterized by progressive optic nerve degeneration. It is currently the leading cause of irreversible blindness worldwide. Recent reports have indicated that neuroinflammation and autophagy are two key factors in glaucoma's neurodegenerative pathological process, where microglia and macroglia are deeply involved.^{7–10} However, the underlying pathogenesis has not been fully elucidated thus far.

Autophagy is a unique life phenomenon of eukaryotic cells, playing important roles in cell growth, development, and aging. It primarily acts to maintain cellular homeostasis under exposure to internal and external stimuli by removing or transforming abnormal proteins, damaged organelles, and other needless substances in cells via lysosome.¹¹ Being a programmed cell death procedure, it behaves as an essential cyclic pathway in neurodegenerative diseases with neuroglia heavily involved.^{12–14}

Müller cell is the most abundant macroglia among the various types of neuroglia in the retina. Müller cells are surrounded by orderly arranged neurons, extending from the ganglion cell layer (GCL) to the photoreceptor inner segment area. Located in a crucial anatomical site, Müller cells may greatly impact basic physiological and pathological conditions.¹⁵ Previous studies have shown that the autophagy of Müller cells is involved in the pathophysiological process of certain ophthalmological diseases, which appear to be strongly linked to neuronal degeneration and survival.^{13,16} How autophagy of Müller cells takes part in

¹Department of Ophthalmology, Ruijin Hospital Affiliated Medical School, Shanghai Jiaotong University, 197 Ruijin Er Road, Shanghai 200025, China

²Department of Ophthalmology, Shanghai General Hospital (Shanghai First People's Hospital), Shanghai Jiao Tong University School of Medicine, Shanghai 200080, China

³Department of Orthopaedics, Shanghai Key Laboratory for Bone and Joint Diseases, Shanghai Institute of Traumatology and Orthopaedics, Ruijin Hospital Affiliated Medical School, Shanghai Jiaotong University, 197 Ruijin Er Road, Shanghai 200025, China

⁴Department of Ophthalmology, Zhoushan Branch of Ruijin Hospital Affiliated Medical School, Shanghai Jiaotong University, Zhoushan, China

⁵These authors contributed equally

⁶Lead contact

*Correspondence: pinghpingh@126.com (P.H.), carl_shen2005@126.com (X.S.), yachtj@hotmail.com (S.H.), yszhong68@126.com (Y.Z.)
<https://doi.org/10.1016/j.isci.2023.106839>



glaucomatous neurodegeneration remains relatively unexplored. We first hypothesized the loss of retinal ganglion cells (RGCs) and the impairment of visual function in glaucoma could be partly attributed to the alteration of Müller cells' autophagic activity. This led to our investigation into the role of Müller cell autophagy in glaucoma in the context of glia interaction, in hopes of understanding the detailed mechanisms of glaucoma pathogenesis to facilitate further studies of therapeutic strategies for glaucoma treatment.

Among the acknowledged autophagy-related proteins, osteopontin (OPN) is a pro-inflammatory cytokine that is secreted and distributed across a wide range of tissues and cells.^{17–20} As a key factor in tissue repairing and extracellular matrix remodeling after injury, OPN has been reported to participate in the pathophysiological processes of several common neurodegenerative diseases and is closely involved in the regulation of autophagy and the consequent impact on neurons.²¹ In the context of eye neurodegenerative disease, OPN was found to be secreted by activated microglia in experimental glaucoma.²² Such activation of innate immune response in different glial cells is also an important mechanism that leads to neuronal damage.²³ Therefore, whether and how the OPN secreted by microglia will affect the autophagy of Müller cells in glaucomatous neurodegeneration, thereby impact the occurrence and development of degenerative neuropathy, has become a question of our concern.

In this study, we investigated the potential molecular signaling roles of OPN in the interaction between retinal microglia and Müller cells. This then forms the basis for understanding the autophagic activity alteration of Müller cells in experimental glaucoma and its related regulatory mechanisms. Insights into microglia-macrogliacrosstalk along with the reciprocal involvement of autophagy in a neurodegenerative context will benefit the exploration of relevant therapeutic strategies targeting neurodegeneration.

RESULTS

OPN overexpression is accompanied by OPN receptors upregulation and autophagy suppression in retinal Müller cells of COH rats

In our previous study, activation and proliferation of microglia along with microglia-derived OPN overexpression were observed in the retina following the induction of COH.²² To further investigate whether and how the microglia-derived OPN plays a signaling role in the autophagic process of Müller cells, in this study we first evaluated the change in retinal OPN level as well as expressions of its receptors and alteration of autophagic activity in retinal Müller cells of COH rats.

OPN secretion levels in the retina just before and 2, 4, and 8 weeks after COH induction were analyzed using ELISA. Results showed that OPN secretion gradually increased as COH maintenance time prolonged, reaching the maximum level after 4 weeks, and began to decrease slightly thereafter ($p < 0.05$) (Figure 1B). The protein and mRNA extracts of rat retina were analyzed with Western blot and RT-PCR to evaluate the expressions of OPN receptors (CD44, Itg α v β 3) and alteration of autophagy activity in the form of related indicators (ATG12, Beclin 1, ATG 5, LC3, and P62) under COH condition. Compared to the control group, the protein expressions of CD44 and Itg α v β 3 in the retina gradually increased as COH maintenance time prolonged ($p < 0.05$) (Figure 1C). Gradual increase in mRNA expression of the receptors was also detected following the induction of COH ($p < 0.05$) (Figure 1D). The autophagy-related proteins (ATG12, Beclin 1, ATG 5, and LC3-II/LC3-I) started to gradually decrease 2 weeks after COH induction, while autophagy substrate P62 increased in parallel ($p < 0.05$) (Figure 1C). The trend of mRNA expressions is basically consistent with that of proteins (Figure 1D), indicating a certain degree of autophagy suppression.

Immunofluorescence was then employed for a more intuitive elucidation of the relationship between OPN receptors in Müller cells, autophagy-related indicators, and the number of RGCs. RGCs are tightly surrounded by Müller cells. Rising CD44/Itg α v β 3 signals, decreasing LC3B signals, and increasing P62 signals in retinal Müller cells along with decreasing RGCs number were observed in COH 4 weeks group when compared with the control group (Figure 1E). In addition, the subcellular structure of the retina was analyzed with a transmission electron microscope. Results showed the number of autophagolysosomes in Müller cells decreased significantly in COH 4 weeks group compared with the control group ($p < 0.05$) (Figure 1F). To further understand the relationship between autophagy in Müller cells and RGCs survival under glaucoma condition, we also assessed the loss of RGCs induced by COH paralleling the above alterations. Retrograde labeling of RGCs showed that the number of surviving RGCs in the group of COH 4 weeks was significantly reduced compared with the sham-operation group (Figure 1G).

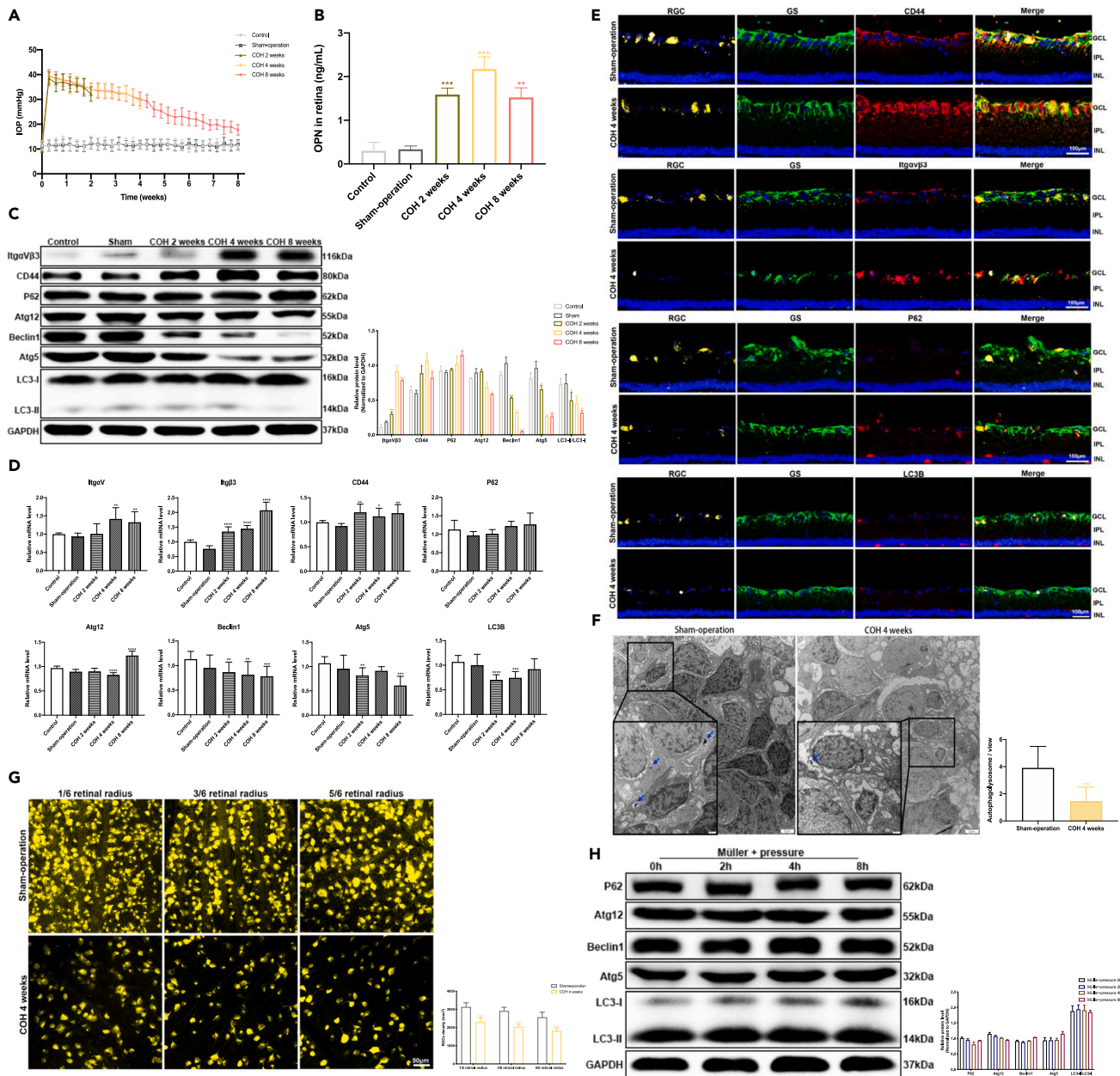


Figure 1. COH induced expression changes in OPN, Itg α v β 3, CD44, P62, Atg12, Beclin 1, Atg5, and LC3 and loss of RGCs

(A) Changes in intraocular pressure (IOP) in rats of control (average, 11.87 ± 2.55 mmHg), sham (average, 12.08 ± 2.62 mmHg), COH 2 weeks (average, 36.60 ± 6.88 mmHg), COH 4 weeks (average, 32.27 ± 8.81 mmHg), COH 8 weeks (average, 25.33 ± 7.31 mmHg) ($n = 15$, Bars represent mean \pm SD).

(B) ELISA analysis of OPN secretion in rat retina 0, 2, 4, and 8 weeks after COH induction ($n = 3$).

(C) Protein expressions of Itg α v β 3, CD44, P62, Atg12, Beclin 1, Atg5, and LC3 in rat retina 0, 2, 4, and 8 weeks after COH induction ($n = 3$).

(D) mRNA expressions of Itg α v β 3, CD44, P62, Atg12, Beclin 1, Atg5, and LC3 in rat retina 0, 2, 4, and 8 weeks after COH induction ($n = 6$).

Bars indicate mean, while error bars show standard deviation.

(E) Triple-labeling of RGCs, GS (specific marker for Müller cells), and Itg α v β 3, CD44, P62, or LC3B in COH retina compared to Sham-operation.

Representative images depict the immunohistochemistry for Itg α v β 3, CD44, P62, or LC3B (red), GS (green), RGCs(gold), and DAPI (blue). (magnification 200, scale bar = 100 μ m).

(F) Representative electron micrographs of autophagic vesicles in the retina of sham-operation and COH 4 weeks rat. (magnification 20000, scale bar = 500 nm).

(G) Retrograde labeling of RGCs with Fluoro-Gold (magnification 200, scale bar = 50 μ m) and quantitative analysis of RGCs counting in retina of Sham-operation and COH groups ($n = 6$).

(H) Protein expressions of P62, Atg12, Beclin 1, Atg5 and LC3 in Müller cells treated with pressure culture for 0, 2, 4, and 8 h ($n = 3$). Data are represented as the mean \pm SD. * $p < 0.05$, ** $p < 0.01$, *** $p < 0.001$, **** $p < 0.0001$ versus the control group.

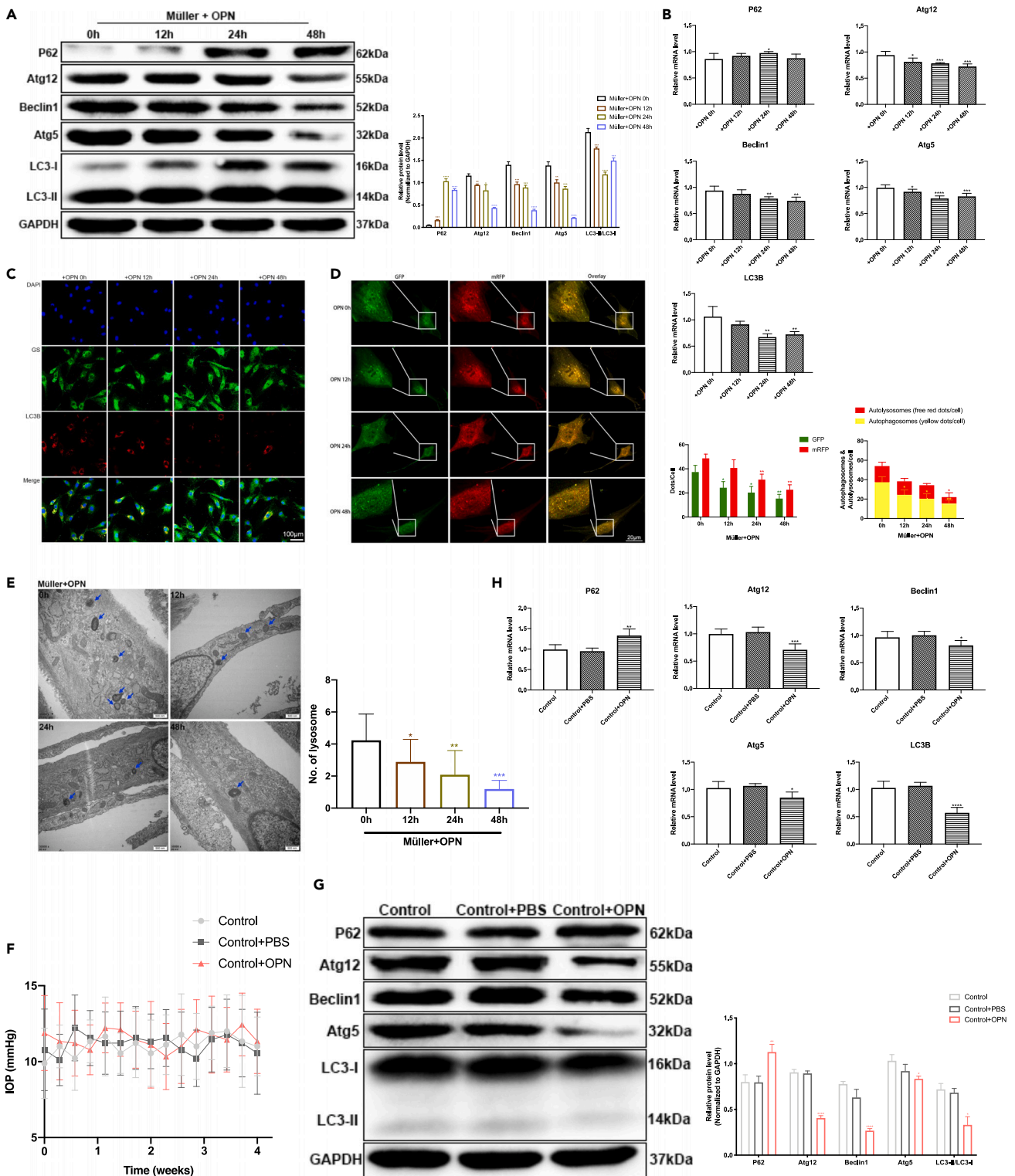


Figure 2. Changes of P62, Atg12, Beclin 1, Atg5 and LC3 expressions in Müller cells treated with OPN

(A) Protein expressions of P62, Atg12, Beclin 1, Atg5, and LC3 in Müller cells treated with OPN for 0, 12, 24, and 48 h (n = 3).

(B) mRNA expressions of P62, Atg12, Beclin 1, Atg5, and LC3 in Müller cells treated with OPN for 0, 12, 24, and 48 h (n = 6). Bars indicate mean, while error bars show standard deviation.

Figure 2. Continued

(C) Double-labeling of GS and LC3B in Müller cells treated with OPN. Representative images depict the immunohistochemistry for LC3B (red), GS (green), and DAPI (blue). magnification 200, scale bar = 100 μ m.

(D) Representative images of Müller cells infected with adenovirus harboring mRFP-GFP-LC3 (magnification 400, scale bar = 20 μ m), and quantitative analysis of LC3 puncta in Müller cells.

(E) Representative electron micrographs of autophagic vesicles in Müller cells treated with OPN. The blue arrows point to the autophagolysosome (magnification 30000, scale bar = 500 nm).

(F) Changes in IOP in rats of control (average, 11.67 \pm 3.04 mmHg), control+PBS (average, 10.78 \pm 3.85 mmHg), control+OPN (average, 11.44 \pm 3.28 mmHg) (n = 9, Bars represent mean \pm SD).

(G) Western blot analysis and densitometry quantification of P62, Atg12, Beclin 1, Atg5, and LC3 in control, sham-operation, and OPN intravitreally injected groups (n = 3).

(H) qRT-PCR analysis of P62, Atg12, Beclin 1, Atg5, and LC3 in control, sham-operation, and OPN intravitreally injected groups (n = 6). Data are represented as the mean \pm SD. *p < 0.05, **p < 0.01, ***p < 0.001, ****p < 0.0001 versus the control group.

The results indicated that the expressions of OPN receptors increased while the autophagic activity was suppressed in retinal Müller cells following the duration of experimental glaucoma, accompanied by a significant loss of RGCs.

Upon the discovery that autophagy levels in Müller cells were reduced in the COH model, we cultured Müller cells under extra pressure *in vitro* and evaluated the corresponding indicators in our preliminary study. However, the results did not show any significant alteration in autophagic activity (Figure 1H). We hypothesized that this inconsistency may be attributed to certain pathophysiological factors of the internal environment of our COH model, which is far more complicated than the condition in pressurized culture media. Considering our findings in previous research²² where microglia are activated to secrete OPN in the same COH model, supported by reports from other researchers highlighting that OPN level closely correlates with autophagic activity in neurodegenerative disease,²¹ we set our sights on the potential relationship between OPN secreted by activated microglia and autophagy in Müller cells under experimental glaucoma condition. We speculated that OPN could downregulate the autophagy activity in Müller cells by binding to OPN receptors on their surfaces and that this process is probably involved in the paralleling lesion of RGCs in experimental glaucoma.

The effect of exogenous OPN on autophagy activity in retinal Müller cells under normal conditions (*in vitro* & *in vivo*)*Exogenous OPN downregulated autophagy activity in primary Müller cells*

To assess the effects of OPN on the autophagy activity in Müller cells, Müller cells were isolated from rat retinas and cultured *in vitro*, then treated with OPN (6.25 μ g/mL) for 0, 12, 24, and 48 h to be observed.

The results of Western blot showed that the level of autophagy-related proteins (ATG12, Beclin 1, ATG 5, and LC3) gradually decreased as the time of OPN treatment increased, while the autophagy substrate P62 gradually accumulated (p < 0.05) (Figure 2A). The trend of mRNAs level changes was consistent with that of proteins correspondingly (p < 0.05) (Figure 2B), indicating that the autophagy level in Müller cells gradually decreased along with the OPN treatment time. In addition, immunofluorescence staining was used to label the LC3 in Müller cells to further demonstrate the changes in autophagy level. The results of immunofluorescence showed that the fluorescence intensity of LC3B in Müller cells gradually weakened as the time of OPN treatment increased (Figure 2C). To assess the variation of autophagic flux, Müller cells were transiently transfected with a plasmid harboring a tandem fluorescent mRFP-GFP-LC3 (tfLC3). GFP degrades in an acidic environment while RFP does not. Thus, yellow spots (formed out of the overlap between red and green) indicate autophagosomes, while red spots indicate autophagic lysosomes. The reduction of yellow spots indicates damage of autophagic flux at the early stage, and if there is damage at the late stage of autophagic flux, only a reduction of red spots will be observed.

The results showed that with the increase of OPN treatment time, the yellow spots and red spots in Müller cells both gradually decreased (p < 0.05) (Figure 2D), indicating that the autophagy flux was damaged at the early stage. Consistently, the results of electron microscopy showed that the amount of autophagolysosome decreased gradually following OPN treatment (p < 0.05) (Figure 2E).

Intravitreal injection of OPN downregulated autophagy activity in retinal Müller cells in normal rats

Subsequently, to verify the results *in vivo*, intravitreal injection of OPN (500 ng/ml) was performed on normal-IOP rats and changes in autophagy activity in the retina were evaluated. Results of qRT-PCR and

Western blot showed that compared with the control group, the level of autophagy activity in the OPN treatment group significantly decreased ($p < 0.05$) (Figures 2G and 2H), indicating that OPN probably suppresses autophagy activity in retinal Müller cells *in vivo* in combination with the above results *in vitro*.

The effect of microglia-derived OPN on autophagy in Müller cells in experimental glaucoma (*in vivo* & *in vitro*)

Intravitreal injection of Anti-OPN and OPN receptor suppressors enhanced autophagy activity in retinal Müller cells and RGCs survival in COH rats

To verify the effects of OPN on retinal autophagy *in vivo*, neutralization of OPN and suppression of OPN receptors were introduced for comparison. Anti-OPN (50 μ M), Anti-CD44 (280 μ g/ml), or selective inhibitor of Itg α V β 3 cyclo RGDyk (cRGDyk, 20 nM) was injected intravitreally before and every other week after COH induction for 4 weeks. The changes of autophagy activity were evaluated after blocking OPN directly or indirectly as mentioned above. In addition, we also observed the survival of RGCs after drug interventions to explore whether the alteration of autophagy in Müller cells was involved in the pathogenesis of glaucoma neuropathy. It was found that, in comparison with the solvent group, the autophagy-related product proteins and mRNAs levels significantly increased, and the autophagy substrate P62 significantly decreased in the three groups that received the intervention of OPN neutralization or OPN receptors suppression, respectively ($p < 0.05$) (Figures 3C, 3D, 4B, 4C, 4F, and 4G).

The results of electron microscopy showed a consistent tendency that the number of autophagolysosome in Müller cells significantly increased in the three groups treated with Anti-OPN, Anti-CD44 or cRGDyk respectively in comparison with the control ($p < 0.05$) (Figures 3E, 4D, and 4H). The retrograde labeling of RGCs showed that compared with the control group, the RGCs survival was significantly enhanced in COH rats treated with either OPN neutralization or OPN receptors suppression ($p < 0.05$) (Figures 3F, 4E, and 4J). The above results indicated significant and synchronous improvement of autophagy activity in retinal Müller cells and RGCs survival in COH rats by blocking the effect of OPN.

Intravitreal injection of minocycline enhanced autophagy activity in Müller cells and RGCs survival in COH rats

To verify the role of microglia-derived OPN in regulating retinal autophagy *in vivo*, rats were intravitreally injected with a specific microglia inhibitor, minocycline, before and every other week after COH induction for 4 weeks. The changes in OPN level, autophagy activity and RGCs survival were then observed after microglia inactivation. It was found that the expressions of Iba-1, CD11b, CD68, OPN were significantly reduced at both protein and mRNA levels in the group treated with minocycline in comparison with the solvent group ($p < 0.05$), indicating that minocycline effectively inhibited the proliferation and activation of microglia, and as a result probably led to downregulation of microglia-derived OPN secretion in COH rats (Figures 5A and 5B).

Simultaneously, the expressions of autophagy-related product increased, and the autophagy substrate P62 decreased at both protein and mRNA levels in COH rats treated with minocycline ($p < 0.05$) (Figures 5C and 5D). The results of electron microscopy showed that autophagolysosome in Müller cells increased significantly in COH rats treated with minocycline in comparison with the control ($p < 0.05$) (Figure 5E). And compared with the PBS group, retrograde labeling presented significant preservation of RGCs in the minocycline groups ($p < 0.05$) (Figure 5F), indicating that inhibiting the activation of microglia could significantly reduce the secretion of microglia-derived OPN, increase the level of autophagy activity in retinal Müller cells, and synchronously reduce the loss of RGCs under experimental glaucoma.

Microglia-derived OPN negatively regulates autophagy activity in primary retinal Müller cells treated with various conditioned culture medium

According to our previous study, release of OPN by microglia can be triggered by pressure stimulus both *in vivo* and *in vitro*, thus in this section, we focused on whether the discrepancy of OPN levels in preconditioned media from microglia cultures under various interventions would impact the autophagic activity in primary retinal Müller cells *in vitro*.

The autophagy activity in isolated primary retinal Müller cells was evaluated after being treated with four different conditioned media from microglia cultures under distinct interventions as following with

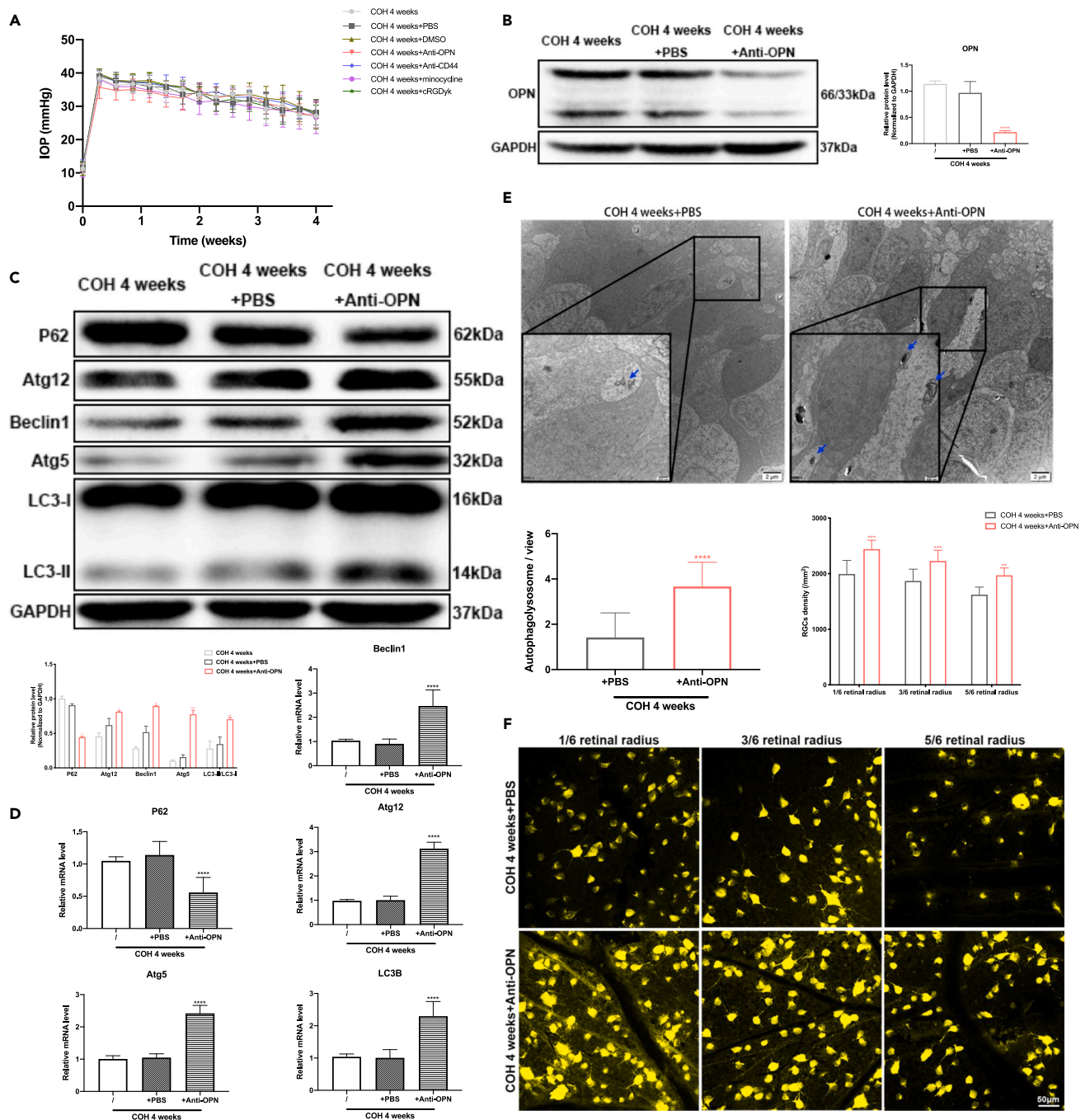


Figure 3. Intravitreally injected Anti-OPN on autophagy of Müller cells in COH rats

(A) Changes in IOP in rats of COH 4 weeks (average, 33.56 ± 6.38 mmHg), COH 4 weeks+ PBS (average, 32.89 ± 5.92 mmHg), COH 4 weeks+ DMSO (average, 33.78 ± 7.54 mmHg), COH 4 weeks + Anti-OPN (average, 31.11 ± 7.32 mmHg), COH 4 weeks + Anti-CD44 (average, 32.09 ± 7.04 mmHg), COH 4 weeks + rRGDyk (average, 31.78 ± 6.67 mmHg), COH 4 weeks + minocycline (average, 32.11 ± 7.15 mmHg) ($n = 9$, Bars represent mean \pm SD).

(B) Western blot analysis and densitometry quantification of OPN in COH, PBS, or Anti-OPN intravitreally injected groups ($n = 3$).

(C) Western blot analysis and densitometry quantification of P62, Atg12, Beclin 1, Atg5, and LC3 in COH, PBS, or Anti-OPN intravitreally injected groups ($n = 3$).

(D) qRT-PCR analysis of P62, Atg12, Beclin 1, Atg5, and LC3 in COH, PBS, or Anti-OPN intravitreally injected groups ($n = 6$).

(E) Representative electron micrographs of autophagic vesicles in retina of PBS or Anti-OPN intravitreally injected groups (magnification 20000, scale bar = 500 nm).

(F) Retrograde labeling of RGCs with Fluoro-Gold (magnification 200, scale bar = 50 μ m), and quantitative analysis of RGCs counting in retina of PBS or Anti-OPN intravitreally injected groups ($n = 6$). Data are represented as the mean \pm SD. * $p < 0.05$, ** $p < 0.01$, *** $p < 0.001$, **** $p < 0.0001$ versus the control group.

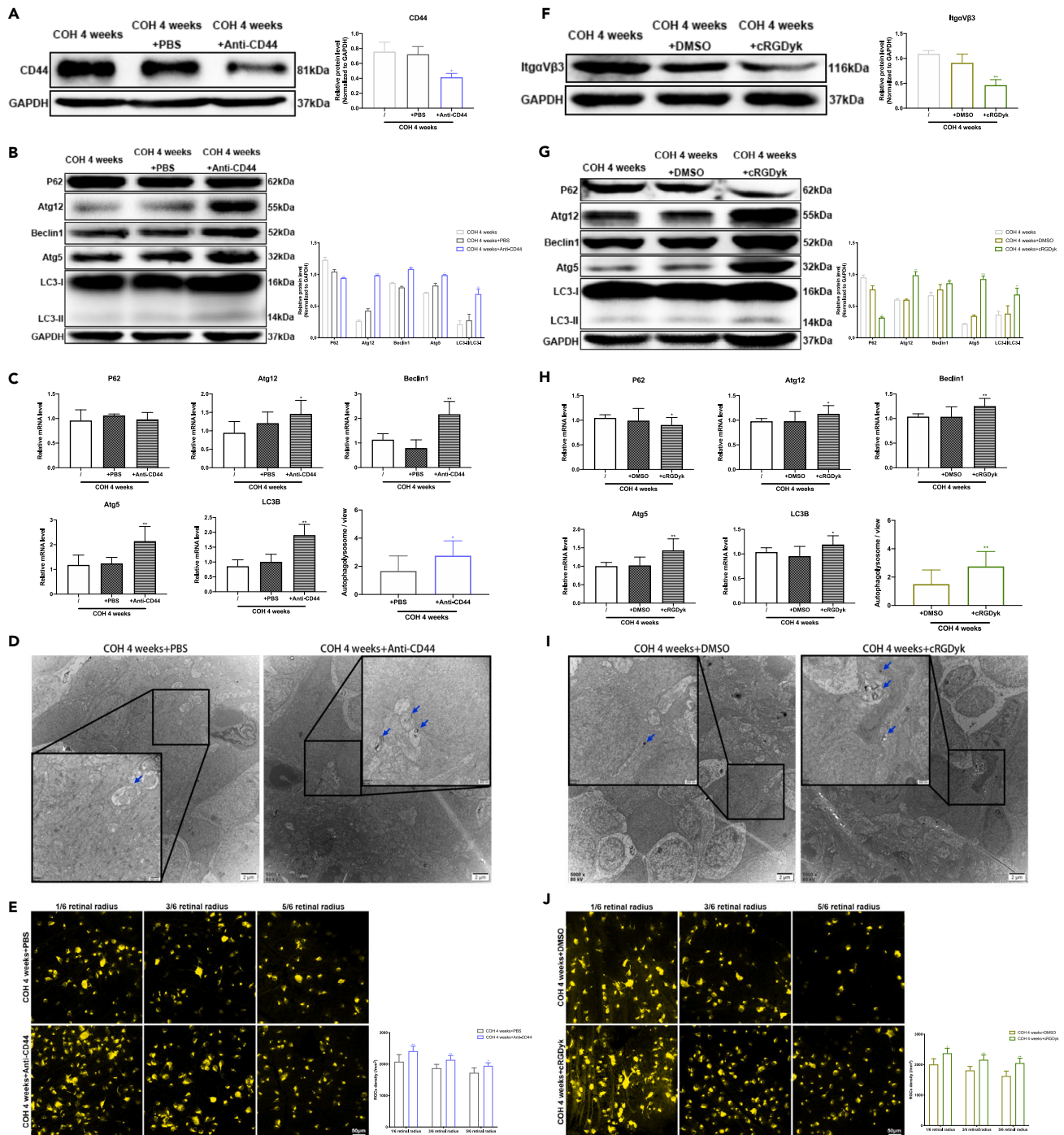


Figure 4. Intravitreally injected inhibitors of OPN receptors (Anti-CD44 or cRGDyk) on autophagy of Müller cells in COH rats
(A–F) Western blot analysis and densitometry quantification of CD44 or ItgaVβ3 in COH, solvent, Anti-CD44, or cRGDyk intravitreally injected groups (n = 3). (B–G) Western blot analysis and densitometry quantification of P62, Atg12, Beclin 1, Atg5, and LC3 in COH, solvent, Anti-CD44, or cRGDyk intravitreally injected groups (n = 3). (C–H) qRT-PCR analysis of P62, Atg12, Beclin 1, Atg5, and LC3 in COH, solvent, Anti-CD44, or cRGDyk intravitreally injected groups (n = 6). (D–I) Representative electron micrographs of autophagic vesicles in retina of solvent, Anti-CD44, or cRGDyk intravitreally injected groups (magnification 20000, scale bar = 500 nm). (E–J) Retrograde labeling of RGCs with Fluoro-Gold (magnification 200, scale bar = 50 μm) and quantitative analysis of RGCs counting in retina of solvent, Anti-CD44, or cRGDyk intravitreally injected groups. Data are represented as the mean ± SD. *p < 0.05, **p < 0.01, ***p < 0.001, ****p < 0.0001 versus the control group.

Figure 5. Continued

(E) Representative electron micrographs of autophagic vesicles in retina of PBS or minocycline intravitreally injected groups (magnification 20000, scale bar = 500 nm).

(F) Retrograde labeling of RGCs with Fluoro-Gold (magnification 200, scale bar = 50 μ m) and quantitative analysis of RGCs counting in retina of PBS or minocycline intravitreally injected groups. Data are represented as the mean \pm SD. * $p < 0.05$, ** $p < 0.01$, *** $p < 0.001$, **** $p < 0.0001$ versus the control group.

respective controls: 1) microglia pretreated with oe-OPN plasmids (oe-OPN vector as control), 2) microglia cultured under pressure (non-pressure as control), 3) microglia transfected with SiR-OPN plasmids then cultured under pressure (SiR-NC then cultured under pressure as control), 4) microglia inactivated by minocycline then cultured under pressure (pretreatment with PBS then cultured under pressure as control).

Compared to the vector control, the OPN content in the culture medium of microglia and the cells per se that were pretreated with oe-OPN plasmids significantly increased according to RT-PCR and ELISA tests ($p < 0.05$) (Figures 6A and 6B). Western blot and RT-PCR showed that the expressions of autophagy-related proteins (ATG12, Beclin 1, ATG 5, and LC3-II/LC3-I) decreased significantly, while autophagy substrate P62 increased obviously in Müller cells treated with this conditioned medium ($p < 0.05$) (Figures 6C and 6D). Consistently, the adenovirus transfection assay of tandem fluorescence probe showed a decrease of yellow and red dots ($p < 0.05$), (Figure 6E), while electron microscopy showed a significant reduction of autophagolysosome number in Müller cells treated with this conditioned medium, indicating lesion of autophagy flux at the early stage in Müller cells exposed to overexpressed microglia-derived OPN ($p < 0.05$) (Figure 6F).

Compared to the non-pressurized control, the OPN content in the culture medium of microglia pressurized for 2, 4, and 8 h gradually increased, reaching peak after 4 h before decline ($p < 0.05$) (Figure 6G). Thus 4 h was chosen as the time point of pressurization duration for microglia culture in subsequent experiments. After being treated with conditioned medium from pressurized microglia culture, the expressions of autophagy-related proteins (ATG12, Beclin 1, ATG 5, and LC3-II/LC3-I) decreased significantly, while the autophagy substrate P62 accumulated markedly in Müller cells ($p < 0.05$) (Figures 6H and 6I). Meanwhile, there was less accumulation of LC3 positive dots ($p < 0.05$) (Figure 6J), and fewer autolysosomes ($p < 0.05$) (Figure 6K) in Müller cells treated with conditioned medium from pressurized microglia culture, indicating lesioned autophagy flux in Müller cells exposed to upregulated microglia-derived OPN in association with pressure stimulus.

Compared to the SiR-NC control, the OPN content in the culture medium of microglia transfected with SiR-OPN plasmids and then pressurized decreased significantly ($p < 0.05$) (Figure 7A). After being treated with conditioned medium from pressurized microglia culture that pretreated with SiR-OPN plasmids, the expressions of autophagy-related proteins (ATG12, Beclin 1, ATG 5, and LC3-II/LC3-I) increased significantly, while the autophagy substrate P62 decreased markedly in Müller cells ($p < 0.05$) (Figures 7B and 7C). Meanwhile, there was an increased accumulation of LC3 positive dots ($p < 0.05$) (Figure 7D), and more amount of autolysosomes ($p < 0.05$) (Figure 7E) in Müller cells treated with this conditioned medium, indicating improvement of autophagy flux in Müller cells probably attributed to downregulation of microglia-derived OPN after gene silence.

Compared to the PBS pretreatment control, the OPN content in the culture medium of microglia pretreated with minocycline and then pressurized decreased significantly ($p < 0.05$) (Figure 7F). After treated with conditioned medium from pressurized microglia culture that was pretreated with minocycline, the expressions of autophagy-related proteins (ATG12, Beclin 1, ATG 5, and LC3-II/LC3-I) increased significantly, while the autophagy substrate P62 decreased markedly in Müller cells ($p < 0.05$) (Figure 7G and H). Meanwhile, there was increased accumulation of LC3 positive dots ($p < 0.05$) (Figure 7I), and more amount of autolysosomes ($p < 0.05$) (Figure 7J) in Müller cells treated with this conditioned medium, indicating improvement of autophagy flux in Müller cells probably attributed to downregulation of microglia-derived OPN after inactivation of microglia.

Overall, results of test 1) and test 2) demonstrated that the autophagy activity in retinal Müller cells was reduced at a higher level of microglia-derived OPN due to pressurization or gene overexpression, while results of test 3) and test 4) demonstrated that opposite results occurred at a lower level of microglia-derived OPN due to gene silence or microglia inactivation.

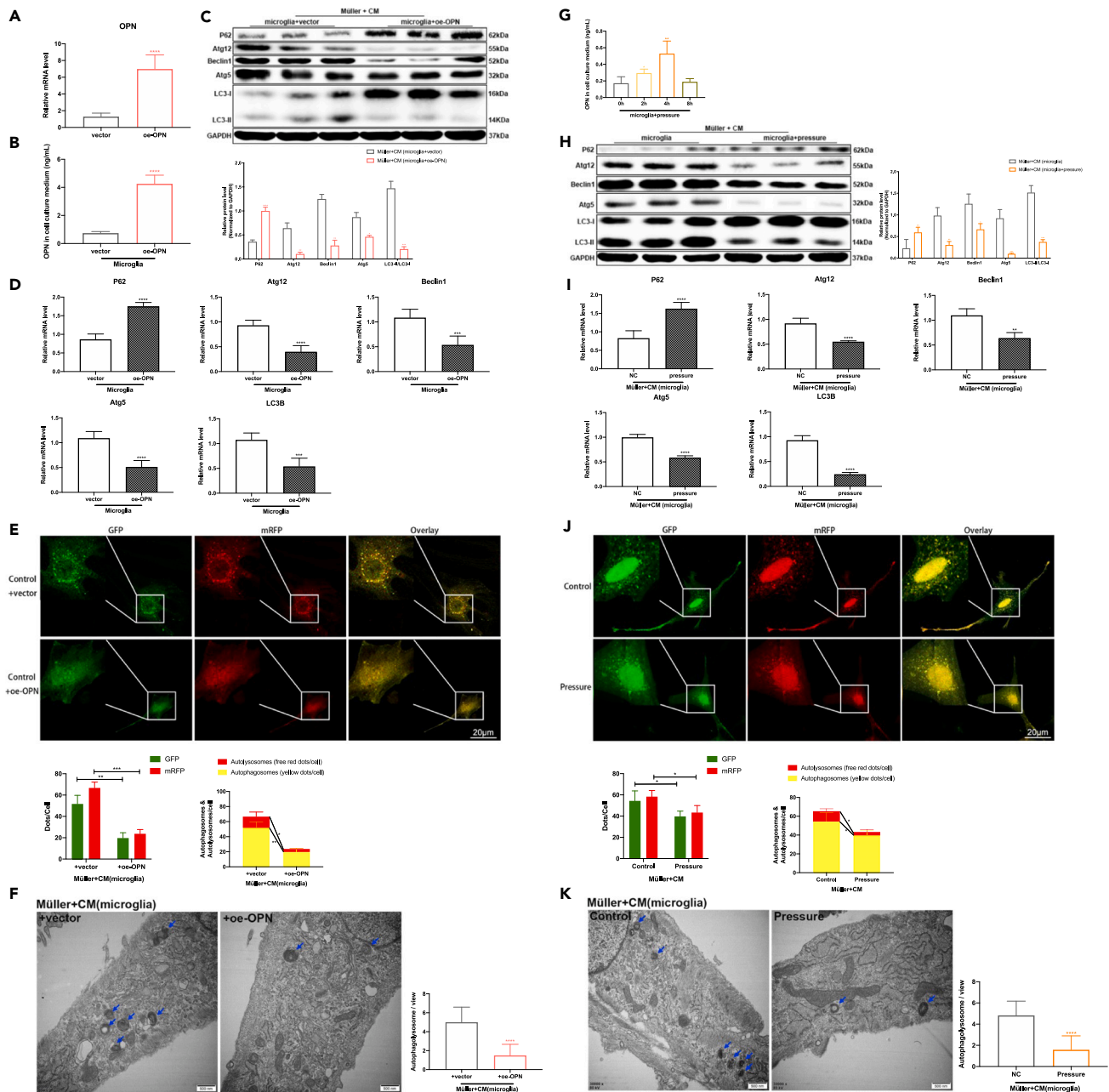


Figure 6. The effects of microglial conditioned culture medium with different treatments (oe-OPN or pressure) on autophagy of Müller cells

(A) qRT-PCR analysis of OPN in microglia treated with vector and oe-OPN (n = 6).

(B–G) The effects of oe-OPN or pressure on release of OPN in microglia (n = 3).

(C–H) Western blot analysis and densitometry quantification of P62, Atg12, Beclin1, Atg5, and LC3B in Müller cells cultured with different microglial conditioned medium (n = 3).

(D–I) qRT-PCR analysis of P62, Atg12, Beclin1, Atg5, and LC3B in Müller cells cultured with different microglial conditioned medium (n = 6).

(E–J) Representative images of Müller cells cultured with different microglial conditioned medium and infected with adenovirus harboring mRFP-GFP-LC3 (magnification 400, scale bar = 20 μm), and quantitative analysis of LC3 puncta in Müller cells (n = 6).

(F–K) Representative electron micrographs and quantitative analysis of autophagic vesicles in Müller cells treated with different microglial conditioned medium. The blue arrows point to lysosome (magnification 30000, scale bar = 500 nm). Data are represented as the mean ± SD. *p < 0.05, **p < 0.01, ***p < 0.001, ****p < 0.0001 versus the control group.

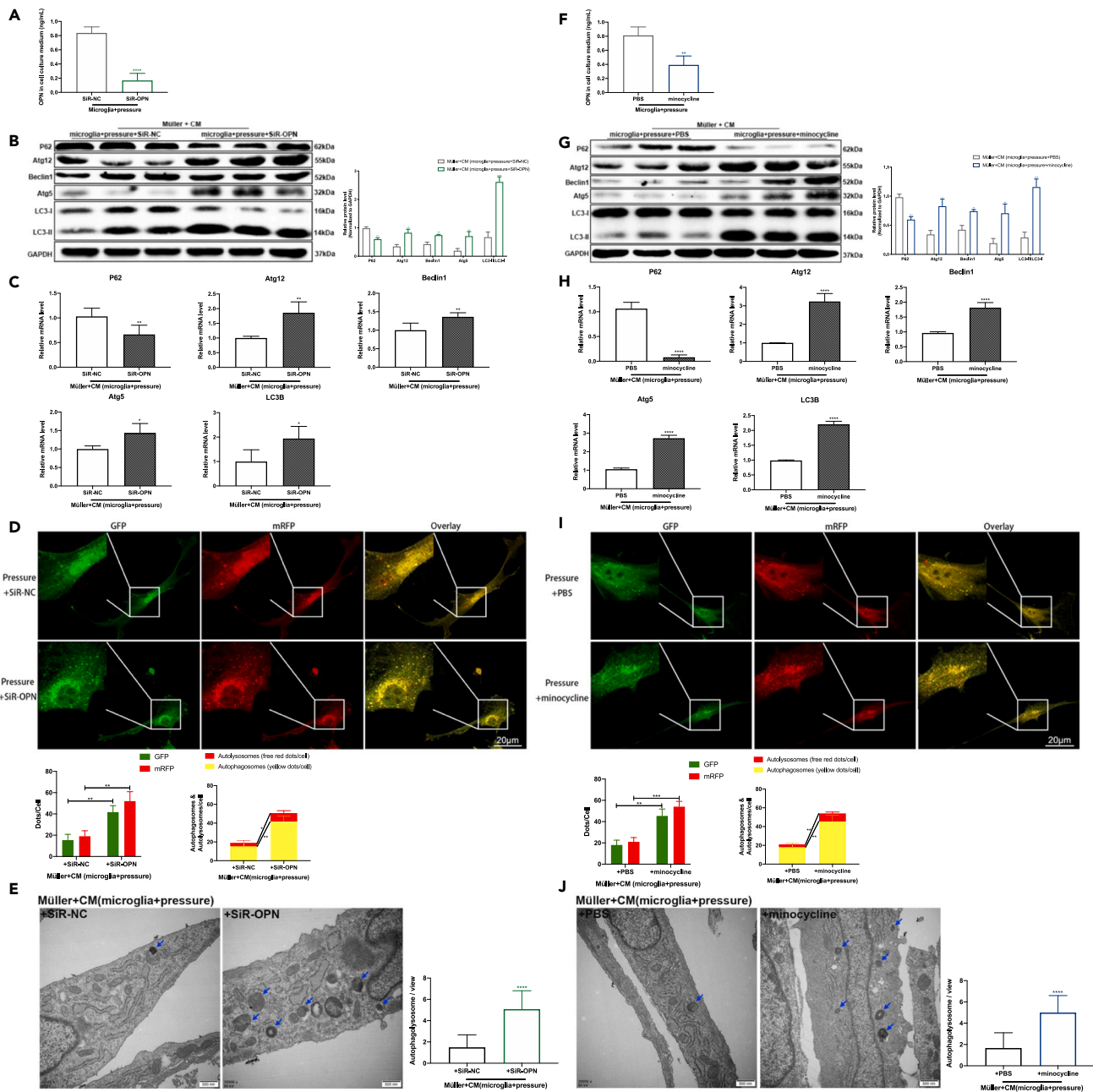


Figure 7. The effects of microglial conditioned culture medium with different treatments (SiR-OPN or minocycline) on autophagy of Müller cells (A–F) The effects of SiR-OPN or minocycline on release of OPN in microglia (n = 3); B, G, Western blot analysis and densitometry quantification of P62, Atg12, Beclin 1, Atg5, and LC3B in Müller cells cultured with different microglial conditioned medium (n = 3); C, H, qRT-PCR analysis of P62, Atg12, Beclin 1, Atg5, and LC3B in Müller cells cultured with different microglial conditioned medium (n = 6); D, I, Representative images of Müller cells cultured with different microglial conditioned medium and infected with adenovirus harboring mRFP-GFP-LC3 (magnification 400, scale bar = 20 μ m), and quantitative analysis of LC3 puncta in Müller cells (n = 6). E, J, Representative electron micrographs and quantitative analysis of autophagic vesicles in Müller cells treated with different microglial conditioned medium (magnification 30000, scale bar = 500 nm). The blue arrows point to lysosome (n = 6). Data are represented as the mean \pm SD. *p < 0.05, **p < 0.01, ***p < 0.001, ****p < 0.0001 versus the control group.

Inhibition of p38 MAPK pathway negatively regulated the effects of microglia-derived OPN on autophagy in retinal Müller cells in experimental glaucoma (*in vitro* and *in vivo*)

Results reported by previous studies have shown that OPN could inhibit autophagy through the p38 MAPK signaling pathway.^{24–26} Inspired by this and based on our preliminary experiments, we treated primary

retinal Müller cells with conditioned medium from microglia culture that pretreated with pressurization or oe-OPN in combination with a p38 MAPK signaling pathway inhibitor SB203580, trying to investigate whether p38 MAPK pathway takes part in the regulation of the interaction between microglia and Müller cells via OPN signaling where autophagy is involved. As results showed, accompanying p-p38 downregulation, the expressions of autophagy-related proteins (ATG12, Beclin 1, ATG 5, and LC3-II/LC3-I) increased significantly, while the autophagy substrate P62 decreased markedly in Müller cells administered with SB203580 and pretreated with either oe-OPN or pressurization ($p < 0.05$) (Figures 8A–8C), indicating the probable involvement of p38 MAPK pathway in the regulation of microglia-derived OPN signaling to Müller cells.

Furthermore, in terms of experiments *in vivo*, SB203580 treatment was performed in rats in combination with intravitreal delivery of OPN or modeling operation of COH. Compared with the control group, the retinal expressions of autophagy-related proteins (ATG12, Beclin 1, ATG 5, and LC3-II/LC3-I) increased significantly, while the autophagy substrate P62 decreased markedly in rats treated with SB203580 in combination with either OPN supplement or COH modeling ($p < 0.05$) (Figures 8E–8G). Taking into account the findings *in vitro* mentioned above, the results presented that p38 MAPK pathway may take part in the regulation of retinal microglia-Müller cells interaction via microglia-derived OPN signaling, where the autophagy in Müller cells is significantly concerned.

DISCUSSION

In the past, neuroglia in CNS was simply regarded as supportive cells to aid neurons in morphologic and neurotrophic terms. However, increasing evidence has emerged, convincing people of the fact that neuroglia, primarily divided into microglia and macroglia, interactively play important roles in the development and pathology courses of the nervous system. Especially in the context of neurodegeneration, microglia and macroglia act as the essential mediators of neuroinflammation, the dynamic alterations of which critically influence the lesion prognosis, involving responses in forms of transcriptome, proteome and functions.^{1–3} Although increasing interests and investigations have focused on the role of microglia-macroglia interaction in the complex context of various neurodegenerative disorders, there still exist a lot of puzzles and challenges to be explored. We in the present study take advantage of established glaucoma models *in vivo* and *in vitro* to try to illustrate some underlying details and mechanisms for this interaction in a neurodegeneration scenario of eye disease, which may introduce certain inspirations to this research field and potential convenience of direct observation through transparent media *in vivo* experiments in further research.

The retina contains three types of glial cells: microglia, astrocytes and Müller cells, with the latter two falling into the macroglia category. The Müller cell is the predominant glial element in the retina, representing 90% of the retinal glia²⁷ and plays a crucial role in regulating and maintaining retinal neuronal functions.²⁸ Microglia is the main cell type that is involved in the immune and inflammatory reactions in glaucoma. It is widely accepted that activated microglia exert dual functions, that is, pro-inflammatory (M1) and anti-inflammatory (M2) effects.²⁹ Cells of Müller glia and microglia both react to neuronal injury in glaucoma. Changes to a reactive phenotype initiate signaling cascades that may play a role in protecting or destroying optic neurons in different pathological stages.³⁰ Previous researchers have found that under normal conditions, Müller cells are potential sources of extracellular ATP that can mediate activity-dependent regulation of microglial dynamic process motility. Morphological, molecular, and functional responses are impacted following microglial activation and signal to Müller cells during inflammation.^{31,32} However, the underlying mechanisms and signaling pathways involved in the crosstalk and the signal cascades between microglia and Müller cells are unclear. More research is needed to help understand the interaction of retinal glial cells and the underlying mechanisms of damage or protection to optic neurons. Discovery of relevant molecular signals, such as OPN, would contribute to the understanding of these multifaceted interactions. Microglia-Müller cell signaling may constitute a target for therapeutic interventions that can direct overall retinal injury responses toward beneficial, and away from detrimental ends.

Autophagy is an evolutionarily conserved intracellular process involved in protein and organelle degradation and has been associated with cell-protective processes as well as cell death.³³ Disruption in autophagy may cause a wide range of human diseases including neurodegenerative diseases, liver diseases, muscle diseases, cardiac diseases, and cancer.³⁴ In recent years, increasing evidence has shown that autophagy plays a role in the pathophysiology of glaucoma, and it is involved in all stages of glaucomatous neuropathy

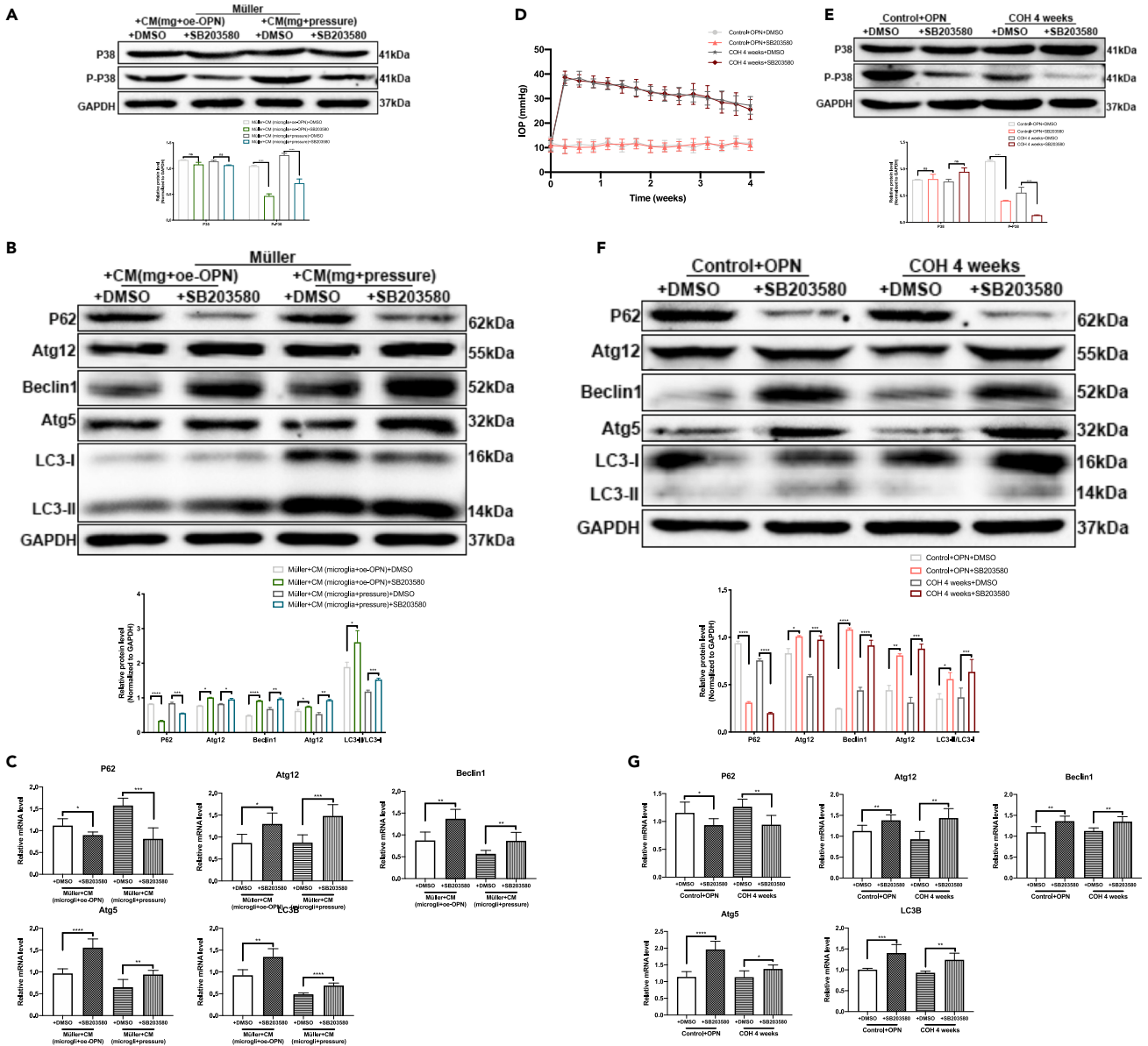


Figure 8. The effects of SB203580 on OPN-induced autophagy of Müller cells *in vitro* and *in vivo*

(A) Western blot analysis and densitometry quantification of p38 and p-p38 in Müller cells treated with OPN+DMSO, OPN+SB203580, pressure+DMSO, pressure +SB203580 (n = 3).

(B) Western blot analysis and densitometry quantification of P62, Atg12, Beclin 1, Atg5, and LC3B in Müller cells treated with OPN+DMSO, OPN+SB203580, pressure+DMSO, pressure +SB203580 (n = 3).

(C) qRT-PCR analysis of P62, Atg12, Beclin 1, Atg5, and LC3B in Müller cells treated with OPN+DMSO, OPN+SB203580, pressure+DMSO, pressure +SB203580 (n = 6).

(D) Changes in IOP in rats of control+OPN+DMSO (average, 11.19 ± 4.87 mmHg), control+OPN+SB203580 (average, 10.96 ± 5.23 mmHg), COH 4 weeks+ DMSO (average, 31.62 ± 6.88 mmHg), COH 4 weeks+ SB203580 (average, 31.43 ± 7.04 mmHg) (n = 12, Bars represent mean \pm SD).

(E) Western blot analysis and densitometry quantification of p38 and p-p38 in retina of control+OPN+DMSO, control+OPN+SB203580, COH 4 weeks+ DMSO, COH 4 weeks + SB203580 groups (n = 3).

(F) Western blot analysis and densitometry quantification of P62, Atg12, Beclin 1, Atg5, and LC3B in retina of control+OPN+DMSO, control+OPN+SB203580, COH 4 weeks+ DMSO, COH 4 weeks + SB203580 groups (n = 3).

(G) qRT-PCR analysis of P62, Atg12, Beclin 1, Atg5 and LC3B in rats' retina of control+OPN+DMSO, control+OPN+SB203580, COH 4 weeks+ DMSO, COH 4 weeks + SB203580 groups (n = 6). Data are represented as the mean \pm SD. *p < 0.05, **p < 0.01, ***p < 0.001, ****p < 0.0001.

processes, where the balance between neuronal death and survival is crux.³⁵ Therefore, restoring autophagy flux may appear to be an efficient therapeutic strategy for this kind of neurodegenerative disease, and hopefully for glaucoma as well,³⁶ which is consistent with the concept proposed in this article. The results of this study suggest that the level of autophagy gradually decreases with the prolonging of the COH modeling time, which is contrary to conclusions from some previous research that autophagy level is to elevate in experimental glaucoma.^{37,38} This discrepancy may be attributed to the differences in modeling mechanisms, the amplitude of IOP elevation, the time point of detection for autophagic activity, most importantly, the difference in the target cell of the study. In addition, we also found a lack of consistency between the protein and mRNA levels of Atg12, P62, and LC3B, particularly at 8 weeks in the COH model. We believe this discrepancy may be due to various factors such as separation of transcription and translation in eukaryotic gene expression, post-transcriptional processing, degradation of transcripts, post-translational processing and modification, and different time points of detection. In the COH model, peak/low point was reached at 8 weeks in terms of degradation/increase of mRNA for Atg12, P62, and LC3B proteins.

The study on autophagy in glaucoma is not rare. However, attention has mostly been focused on the changes of autophagy in the trabecular meshwork (TM), microglia, astrocytes, and especially RGCs. Porter et al.³⁹ indicated that the decreased autophagic flux (an indicator of autophagic activity) caused by oxidative stress may be one of the factors that lead to the progressive failure of cellular TM function with age and may be partially responsible for the pathogenesis of primary open-angle glaucoma (POAG). Su et al.⁴⁰ demonstrated that the autophagy activator rapamycin significantly inhibits the expression of Iba-1 (a specific marker for activated microglia) and enhanced the expression of NF- κ B in a rat model of COH. Additionally, Tezel et al.⁴¹ reported a marked upregulation of mTOR, Atg3, and Atg7 in retinal astrocytes in an experimental rat model of glaucoma, which indicated participation of autophagic pathway in the activation of neuroinflammation under glaucoma condition. In terms of neuronal issues, Park et al.⁴² confirmed that autophagosomes are deposited in the dendrites of RGCs in a chronic hypertensive glaucoma rat model and that autophagy is activated earlier in the dendrites of RGCs than in the cytoplasm of RGCs. However, the autophagy of Müller cells, which plays an important role in the progress of glaucoma, has not received much attention. Therefore, there is plenty of space to explore on the topic of changes in autophagy of Müller cells and related mechanisms in glaucoma. The present study took on the significance to fill the gap in this research field.

Reactive Müller cells have been found in the retina of glaucoma patients.⁴³ Activation of Müller cells was also observed in DBA/2J mouse (a kind of inherited glaucoma model) at a very early stage, suggesting that Müller cells play an important role in the pathogenesis of glaucoma.⁴⁴ Kang et al.¹⁶ found that the autophagy of Müller cells was closely related to the apoptosis of RGCs in the optic nerve injury model, which is consistent with the findings in the present research. Wang et al.⁴⁵ reported that the downregulation of autophagy in Müller cells destroyed lysosome function, increased apoptosis, and impaired cell function. Lopes et al.⁴⁶ found that autophagic malfunction of Müller cells can lead to a massive VEGF production and an increased apoptotic rate, which may lead to a breakdown of the blood-retinal barrier and neurodegeneration. As main sources of ATP and neurotrophic factors, Müller cells provide energy and nutrients for the physiological activities of RGCs.^{47,48} Studies have reported that extracellular ATP levels are significantly elevated in the retina of glaucoma patients and DBA/2J mice.^{49,50} Reactive Müller cells exhibit greater responses to extracellular stimuli and therefore release more ATP, which may induce RGCs damage through activation of RGCs-expressed P2X7 receptors.⁵¹ In addition, glutamate is an important intraretinal excitatory neurotransmitter that transmits visual information from photoreceptors to RGCs. K⁺ channel (Kir4.1) function in Müller cells is significantly impaired under conditions of high intraocular pressure.⁵² The decrease in Kir4.1 channel activity causes the accumulation of extracellular glutamate.⁵³ Elevated extracellular K⁺ level triggers neuronal excitation, glutamate release, and excitotoxicity resulting in a marked loss of RGCs. These reports suggest that disruption of autophagy in Müller cells contributes to cellular dysfunction, and the impairment of Müller cell physiological function may trigger RGCs lesion under various pathological circumstances. Therefore, we have reason to speculate that the downregulation of autophagy in Müller cells may indirectly affect RGCs survival due to alterations in their normal supportive functions under glaucomatous conditions. Of course, this hypothesis needs further experiments for verification.

This study attempts to demonstrate the scientific hypotheses (microglia-OPN-P38 MAPK-Müller cell autophagy-RGCs loss) from various aspects. *In vitro* experiments showed that this pathway affects the

autophagy flow activity of Müller cells by regulating the interaction chain between microglia and OPN in the case of irrelevant RGCs ecology, while *in vivo* experiments introduced a complex network of relationships between RGCs and other retinal cells. The direct impact of microglial activation or OPN on RGCs or other cells cannot be ruled out, but combined with the results obtained from the observation of the relationship between microglia and Müller cells under the control of *in vitro* experimental conditions, as well as the previous research on OPN in the *in vivo* experimental stage for RGCs, we think that the microglia-OPN-P38 MAPK-Müller cell autophagy chain at least partly and significantly contribute to RGCs survival.

OPN can be divided into subtypes of intracellular OPN (iOPN, in the nucleus) and secreted OPN (sOPN, in the cytoplasm).^{54,55} The sOPN works by binding to the extracellular receptors expressed by the target cells while the iOPN acts by binding to MyD88, which is located downstream of the toll-like receptor.⁵⁶ *In vivo*, both the two kinds of OPN can play a part in the immune regulation process through different pathways. OPN mentioned in the present study only refers to the sOPN, which is a defect of this research. The important role of iOPN should not be ignored in future research. OPN receptors include integrins and CD44 families.^{57,58} OPN has two critical integrin-binding sequences: arginine-glycine-aspartic acid (RGD) and serine-valine-valine-tyrosine-glutamate-leucine-arginine (SVVYGLR). OPN interacts mainly with various α (particularly α v β 1, α v β 3, α v β 5) integrin receptors via the classical RGD sequence, and interacts with α 9 β 1, α 4 β 1, α 4 β 7 via SVVYGLR.^{59–61} It also interacts with the CD44 via the C-terminal fragment calcium-binding site.^{62–64} Here, we found that CD44 and Itg α v β 3 were both involved in the regulation of OPN on autophagy, which is not completely consistent with the previous research results of Liu et al.¹⁹ Thus, we speculate that OPN may regulate cell autophagy differently dependent on cell type and disease characteristics, and the temporal features of initiating and enduring may also matter.

Limitations of the study

Limitations of our study include the absence of *in vivo* experiments on OPN knockout or overexpression rats. This was mostly due to time constraints and resource scarcity in terms of rat breed featuring retina-specific OPN deleted or overexpressed, and we alternatively adopted the method of using OPN knock-down and overexpression microglia *in vitro*. The present study also only focused on microglia interaction with macroglia Müller cells. Macroglia astrocytes, though present in small numbers in the retina, were not covered. We plan to study this area in the near future by breeding rats with specific gene types to ensure a rigorous experimental design.

Comprehensively, the direct evidence provided in this study suggested that microglia-derived OPN was upregulated while autophagy level in Müller cells decreased significantly along with RGCs loss in rat glaucoma model. *In vitro* experiments further confirmed the correlation between inhibition of autophagy in Müller cells and microglia-derived OPN via the activation of its receptors integrin α v β 3/CD44 and mediation of p38 MAPK signaling pathway. OPN appears to be a novel discovered molecular signaling pathway for microglia-macroglia interaction in the neurodegenerative scenario of glaucoma, and the reduced autophagy in Müller cells caused by microglia-derived OPN may contribute to the loss of neuronal cells in experimental glaucoma (Figure 9). Whether the situation also coincides in CNS warrants further validation. Undoubtedly, it may serve as a potential target for treatment of glaucoma and other neurodegenerative diseases, and modulation of neural pathophysiology through regulating interactive signals between different types of glial cells is expected to become a research direction for exploring new therapeutic strategies in the field of neurodegeneration.

STAR★METHODS

Detailed methods are provided in the online version of this paper and include the following:

- KEY RESOURCES TABLE
- RESOURCE AVAILABILITY
 - Lead contact
 - Materials availability
 - Data and code availability
- EXPERIMENTAL MODEL AND SUBJECT DETAILS
 - Animals
 - Primary rat retinal microglia cultures
 - Primary rat Müller cells cultures

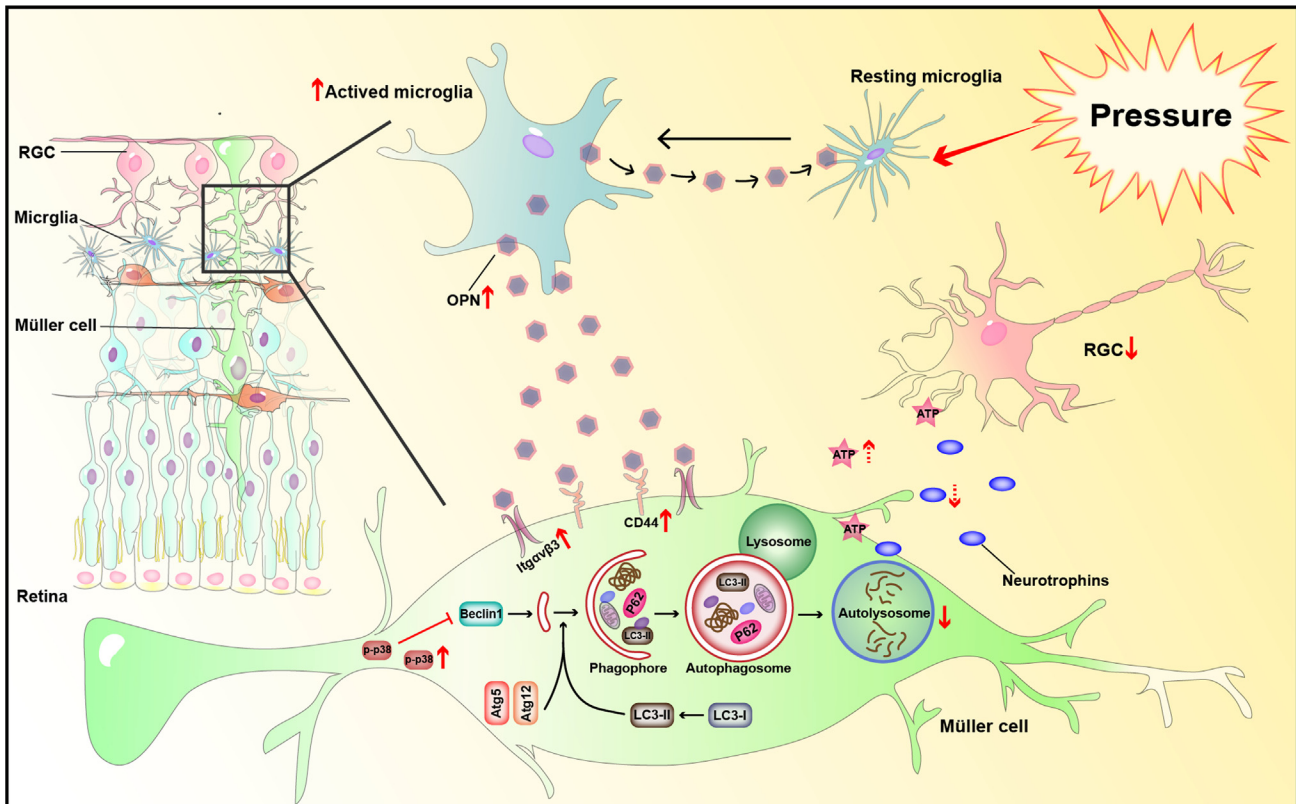


Figure 9. The crosstalk between microglia, Müller cells and RGCs in retina under pressure

In the context of experimental glaucoma, the increase in intraocular pressure stimulates retinal microglia to activate and secrete an abundance of OPN. OPN that is highly expressed down-regulates Müller autophagy by binding to the receptor CD44/Igαvβ3 on the surface of Müller cells. This affects their normal life activities, energy, and nutrient supply, which ultimately increases RGCs loss. The p38-MAKP signaling pathway plays a significant regulatory role in this process.

● METHOD DETAILS

- Anesthesia of rats
- Induction of IOP elevation
- IOP measurement
- Intravitreal injection
- Retrograde labeling and quantification of RGCs
- Cell treatments with OPN
- Transfection of siRNA
- Plasmids transfection and transient expression of OPN
- Preparation of three-dimensional matrigel matrix
- Pressure loading of cell cultures
- Transfection of Ad-CMV-RFP-GFP-LC3 and evaluation of fluorescent LC3 puncta
- Transmission electron microscope
- Immunofluorescence
- Western blot analysis
- Quantitative real-time RT-PCR

● QUANTIFICATION AND STATISTICAL ANALYSIS

ACKNOWLEDGMENTS

Funding: National Natural Science Foundation of China [NO. 81870652], National Natural Science Foundation of China [NO. 82070953], National Natural Science Foundation of China [NO. 82000885], Shanghai Science and Technology Committee Project Foundation [NO. 16411961900], Shanghai Science and

Technology Committee Project Foundation [NO. 17140903000] Shanghai Municipal Commission of Health and Family Planning Project Foundation [NO. 2020LP034], Shanghai Municipal Commission of Health and Family Planning Project Foundation [NO. 2018JP008], Natural Science Foundation of Shanghai [NO. 21ZR1439700], Ruijin Youth NSFC Cultivation Foundation [NO. 2019QNYPY01026].

AUTHOR CONTRIBUTIONS

H.Y.: Conceptualization, Methodology, Writing-Original Draft; H.Z.: Validation, Methodology, Data analysis; J.S.: Investigation, Validation; N.L.: Software, Data analysis; J.C.: Investigation; B.S.: Statistics; P.H.: Supervision; X.S.: Resources, Project administration; S.H. & Y.Z.: Conceptualization, Funding acquisition, Writing - Review & Editing. All authors have read and agreed to the published version of the manuscript.

DECLARATION OF INTERESTS

Authors declare that they have no competing interests.

Received: September 14, 2022

Revised: February 1, 2023

Accepted: May 4, 2023

Published: May 9, 2023

REFERENCES

- Chu, T., Shields, L.B.E., Zeng, W., Zhang, Y.P., Wang, Y., Barnes, G.N., Shields, C.B., and Cai, J. (2021). Dynamic glial response and crosstalk in demyelination-remyelination and neurodegeneration processes. *Neural Regen. Res.* 16, 1359–1368. <https://doi.org/10.4103/1673-5374.300975>.
- Matejuk, A., and Ransohoff, R.M. (2020). Crosstalk between astrocytes and microglia: an overview. *Front. Immunol.* 11, 1416. <https://doi.org/10.3389/fimmu.2020.01416>.
- Liddelwell, S.A., Marsh, S.E., and Stevens, B. (2020). Microglia and astrocytes in disease: dynamic duo or partners in crime? *Trends Immunol.* 41, 820–835. <https://doi.org/10.1016/j.it.2020.07.006>.
- Liddelwell, S.A., Guttenplan, K.A., Clarke, L.E., Bennett, F.C., Bohlen, C.J., Schirmer, L., Bennett, M.L., Münch, A.E., Chung, W.S., Peterson, T.C., et al. (2017). Neurotoxic reactive astrocytes are induced by activated microglia. *Nature* 541, 481–487. <https://doi.org/10.1038/nature21029>.
- Hong, S., Beja-Glasser, V.F., Nfonoyim, B.M., Frouin, A., Li, S., Ramakrishnan, S., Merry, K.M., Shi, Q., Rosenthal, A., Barres, B.A., et al. (2016). Complement and microglia mediate early synapse loss in Alzheimer mouse models. *Science* 352, 712–716. <https://doi.org/10.1126/science.aad8373>.
- Litvinchuk, A., Wan, Y.W., Swartzlander, D.B., Chen, F., Cole, A., Propson, N.E., Wang, Q., Zhang, B., Liu, Z., and Zheng, H. (2018). Complement C3aR inactivation attenuates tau pathology and reverses an immune network deregulated in tauopathy models and Alzheimer's disease. *Neuron* 100, 1337–1353.e5. <https://doi.org/10.1016/j.neuron.2018.10.031>.
- Hirt, J., Porter, K., Dixon, A., McKinnon, S., and Liton, P.B. (2018). Contribution of autophagy to ocular hypertension and neurodegeneration in the DBA/2J spontaneous glaucoma mouse model. *Cell Death Dis.* 4, 14. <https://doi.org/10.1038/s41420-018-0077-y>.
- Rodríguez-Muela, N., Germain, F., Mariño, G., Fitz, P.S., and Boya, P. (2012). Autophagy promotes survival of retinal ganglion cells after optic nerve axotomy in mice. *Cell Death Differ.* 19, 162–169. <https://doi.org/10.1038/cdd.2011.88>.
- Deng, S., Wang, M., Yan, Z., Tian, Z., Chen, H., Yang, X., and Zhuo, Y. (2013). Autophagy in retinal ganglion cells in a rhesus monkey chronic hypertensive glaucoma model. *PLoS One* 8, e77100. <https://doi.org/10.1371/journal.pone.0077100>.
- Porter, K.M., Jeyabalan, N., and Liton, P.B. (2014). MTOR-independent induction of autophagy in trabecular meshwork cells subjected to biaxial stretch. *Biochim. Biophys. Acta* 1843, 1054–1062. <https://doi.org/10.1016/j.bbamac.2014.02.010>.
- Olzsha, H., Schermann, S.M., Woerner, A.C., Pinkert, S., Hecht, M.H., Tartaglia, G.G., Vendruscolo, M., Hayer-Hartl, M., Hartl, F.U., and Vabulas, R.M. (2011). Amyloid-like aggregates sequester numerous metastable proteins with essential cellular functions. *Cell* 144, 67–78. <https://doi.org/10.1016/j.cell.2010.11.050>.
- Glick, D., Barth, S., and Macleod, K.F. (2010). Autophagy: cellular and molecular mechanisms. *J. Pathol.* 221, 3–12. <https://doi.org/10.1002/path.2697>.
- Ao, H., Li, H., Zhao, X., Liu, B., and Lu, L. (2021). TXNIP positively regulates the autophagy and apoptosis in the rat Müller cell of diabetic retinopathy. *Life Sci.* 267, 118988. <https://doi.org/10.1016/j.lfs.2020.118988>.
- Guo, F., Liu, X., Cai, H., and Le, W. (2018). Autophagy in neurodegenerative diseases: pathogenesis and therapy. *Brain Pathol.* 28, 3–13. <https://doi.org/10.1111/bpa.12545>.
- Wang, Y., Liu, X., Zhu, L., Li, W., Li, Z., Lu, X., Liu, J., Hua, W., Zhou, Y., Gu, Y., and Zhu, M. (2020). PG545 alleviates diabetic retinopathy by promoting retinal Müller cell autophagy to inhibit the inflammatory response. *Biochem. Biophys. Res. Commun.* 531, 452–458. <https://doi.org/10.1016/j.bbrc.2020.07.134>.
- Kang, L.H., Zhang, S., Jiang, S., and Hu, N. (2019). Activation of autophagy in the retina after optic nerve crush injury in rats. *Int. J. Ophthalmol.* 12, 1395–1401. <https://doi.org/10.18240/ijo.2019.09.04>.
- Denhardt, D.T., and Guo, X. (1993). Osteopontin: a protein with diverse functions. *Faseb. J.* 7, 1475–1482.
- Sun, C.M., Enkhjargal, B., Reis, C., Zhou, K.R., Xie, Z.Y., Wu, L.Y., Zhang, T.Y., Zhu, Q.Q., Tang, J.P., Jiang, X.D., and Zhang, J.H. (2019). Osteopontin attenuates early brain injury through regulating autophagy-apoptosis interaction after subarachnoid hemorrhage in rats. *CNS Neurosci. Ther.* 25, 1162–1172. <https://doi.org/10.1111/cns.13199>.
- Liu, G., Fan, X., Tang, M., Chen, R., Wang, H., Jia, R., Zhou, X., Jing, W., Wang, H., Yang, Y., et al. (2016). Osteopontin induces autophagy to promote chemo-resistance in human hepatocellular carcinoma cells. *Cancer Lett.* 383, 171–182. <https://doi.org/10.1016/j.canlet.2016.09.033>.
- Huang, R.H., Quan, Y.J., Chen, J.H., Wang, T.F., Xu, M., Ye, M., Yuan, H., Zhang, C.J., Liu, X.J., and Min, Z.J. (2017). Osteopontin promotes cell migration and invasion, and inhibits apoptosis and autophagy in colorectal cancer by activating the p38 MAPK signaling pathway. *Cell. Physiol. Biochem.* 41, 1851–1864. <https://doi.org/10.1159/000471933>.
- Ulland, T.K., Song, W.M., Huang, S.C.C., Ulrich, J.D., Sergushichev, A., Beatty, W.L., Loboda, A.A., Zhou, Y., Cairns, N.J., Kambal, A., et al. (2017). TREM2 maintains microglial

- metabolic fitness in alzheimer's disease. *Cell* 170, 649–663.e13. <https://doi.org/10.1016/j.cell.2017.07.023>.
22. Yu, H., Zhong, H., Li, N., Chen, K., Chen, J., Sun, J., Xu, L., Wang, J., Zhang, M., Liu, X., et al. (2021). Osteopontin activates retinal microglia causing retinal ganglion cells loss via p38 MAPK signaling pathway in glaucoma. *Faseb. J.* 35, e21405. <https://doi.org/10.1096/fj.202002218R>.
 23. Joshi, A.U., Minhas, P.S., Liddelov, S.A., Hailelessie, B., Andreasson, K.I., Dorn, G.W., 2nd, and Mochly-Rosen, D. (2019). Fragmented mitochondria released from microglia trigger A1 astrocytic response and propagate inflammatory neurodegeneration. *Nat. Neurosci.* 22, 1635–1648. <https://doi.org/10.1038/s41593-019-0486-0>.
 24. Kim, D.S., Kim, J.H., Lee, G.H., Kim, H.T., Lim, J.M., Chae, S.W., Chae, H.J., and Kim, H.R. (2010). p38 Mitogen-activated protein kinase is involved in endoplasmic reticulum stress-induced cell death and autophagy in human gingival fibroblasts. *Biol. Pharm. Bull.* 33, 545–549. <https://doi.org/10.1248/bpb.33.545>.
 25. He, Y., She, H., Zhang, T., Xu, H., Cheng, L., Yepes, M., Zhao, Y., and Mao, Z. (2018). p38 MAPK inhibits autophagy and promotes microglial inflammatory responses by phosphorylating ULK1. *J. Cell Biol.* 217, 315–328. <https://doi.org/10.1083/jcb.201701049>.
 26. Simone, C. (2007). Signal-dependent control of autophagy and cell death in colorectal cancer cell: the role of the p38 pathway. *Autophagy* 3, 468–471. <https://doi.org/10.4161/auto.4319>.
 27. Vecino, E., Rodriguez, F.D., Ruzafa, N., Pereiro, X., and Sharma, S.C. (2016). Glia-neuron interactions in the mammalian retina. *Prog. Retin. Eye Res.* 51, 1–40. <https://doi.org/10.1016/j.preteyeres.2015.06.003>.
 28. Bringmann, A., Pannicke, T., Grosche, J., Francke, M., Wiedemann, P., Skatchkov, S.N., Osborne, N.N., and Reichenbach, A. (2006). Müller cells in the healthy and diseased retina. *Prog. Retin. Eye Res.* 25, 397–424. <https://doi.org/10.1016/j.preteyeres.2006.05.003>.
 29. Kobayashi, K., Imagama, S., Ohgomori, T., Hirano, K., Uchimura, K., Sakamoto, K., Hirakawa, A., Takeuchi, H., Suzumura, A., Ishiguro, N., and Kadomatsu, K. (2013). Minocycline selectively inhibits M1 polarization of microglia. *Cell Death Dis.* 4, e525. <https://doi.org/10.1038/cddis.2013.54>.
 30. Seitz, R., Ohlmann, A., and Tamm, E.R. (2013). The role of Müller glia and microglia in glaucoma. *Cell Tissue Res.* 353, 339–345. <https://doi.org/10.1007/s00441-013-1666-y>.
 31. Wang, M., and Wong, W.T. (2014). Microglia-Müller cell interactions in the retina. *Adv. Exp. Med. Biol.* 801, 333–338. https://doi.org/10.1007/978-1-4614-3209-8_42.
 32. Conedera, F.M., Pousa, A.M.Q., Mercader, N., Tschopp, M., and Enzmann, V. (2019). Retinal microglia signaling affects Müller cell behavior in the zebrafish following laser injury induction. *Glia* 67, 1150–1166. <https://doi.org/10.1002/glia.23601>.
 33. Mizushima, N., Levine, B., Cuervo, A.M., and Klionsky, D.J. (2008). Autophagy fights disease through cellular self-digestion. *Nature* 451, 1069–1075. <https://doi.org/10.1038/nature06639>.
 34. Levine, B., and Kroemer, G. (2008). Autophagy in the pathogenesis of disease. *Cell* 132, 27–42. <https://doi.org/10.1016/j.cell.2007.12.018>.
 35. Munemasa, Y., and Kitaoka, Y. (2015). Autophagy in axonal degeneration in glaucomatous optic neuropathy. *Prog. Retin. Eye Res.* 47, 1–18. <https://doi.org/10.1016/j.preteyeres.2015.03.002>.
 36. Harris, H., and Rubinshtein, D.C. (2011). Control of autophagy as a therapy for neurodegenerative disease. *Nat. Rev. Neurol.* 8, 108–117. <https://doi.org/10.1038/nrneurol.2011.200>.
 37. Produit-Zengaffinen, N., Pournaras, C.J., and Schorderet, D.F. (2014). Autophagy induction does not protect retina against apoptosis in ischemia/reperfusion model. *Adv. Exp. Med. Biol.* 801, 677–683. https://doi.org/10.1007/978-1-4614-3209-8_85.
 38. Wei, T., Kang, Q., Ma, B., Gao, S., Li, X., and Liu, Y. (2015). Activation of autophagy and paraptosis in retinal ganglion cells after retinal ischemia and reperfusion injury in rats. *Exp. Ther. Med.* 9, 476–482. <https://doi.org/10.3892/etm.2014.2084>.
 39. Porter, K., Nallathambi, J., Lin, Y., and Liton, P.B. (2013). Lysosomal basification and decreased autophagic flux in oxidatively stressed trabecular meshwork cells: implications for glaucoma pathogenesis. *Autophagy* 9, 581–594. <https://doi.org/10.4161/auto.23568>.
 40. Su, W., Li, Z., Jia, Y., and Zhuo, Y. (2014). Rapamycin is neuroprotective in a rat chronic hypertensive glaucoma model. *PLoS One* 9, e99719. <https://doi.org/10.1371/journal.pone.0099719>.
 41. Tezel, G., Yang, X., Luo, C., Cai, J., and Powell, D.W. (2012). An astrocyte-specific proteomic approach to inflammatory responses in experimental rat glaucoma. *Invest. Ophthalmol. Vis. Sci.* 53, 4220–4233. <https://doi.org/10.1167/iovs.11-9101>.
 42. Park, H.Y.L., Kim, J.H., and Park, C.K. (2012). Activation of autophagy induces retinal ganglion cell death in a chronic hypertensive glaucoma model. *Cell Death Dis.* 3, e290. <https://doi.org/10.1038/cddis.2012.26>.
 43. Tezel, G., Chauhan, B.C., LeBlanc, R.P., and Wax, M.B. (2003). Immunohistochemical assessment of the glial mitogen-activated protein kinase activation in glaucoma. *Invest. Ophthalmol. Vis. Sci.* 44, 3025–3033. <https://doi.org/10.1167/iovs.02-1136>.
 44. Inman, D.M., and Horner, P.J. (2007). Reactive nonproliferative gliosis predominates in a chronic mouse model of glaucoma. *Glia* 55, 942–953. <https://doi.org/10.1002/glia.20516>.
 45. Wang, L., Sun, X., Zhu, M., Du, J., Xu, J., Qin, X., Xu, X., and Song, E. (2019). Epigallocatechin-3-gallate stimulates autophagy and reduces apoptosis levels in retinal Müller cells under high-glucose conditions. *Exp. Cell Res.* 380, 149–158. <https://doi.org/10.1016/j.yexcr.2019.04.014>.
 46. Lopes de Faria, J.M., Duarte, D.A., Montemurro, C., Papadimitriou, A., Consonni, S.R., and Lopes de Faria, J.B. (2016). Defective autophagy in diabetic retinopathy. *Invest. Ophthalmol. Vis. Sci.* 57, 4356–4366. <https://doi.org/10.1167/iovs.16-19197>.
 47. Bringmann, A., Landiev, I., Pannicke, T., Wurm, A., Hollborn, M., Wiedemann, P., Osborne, N.N., and Reichenbach, A. (2009). Cellular signaling and factors involved in Müller cell gliosis: neuroprotective and detrimental effects. *Prog. Retin. Eye Res.* 28, 423–451. <https://doi.org/10.1016/j.preteyeres.2009.07.001>.
 48. Newman, E.A., and Zahs, K.R. (1998). Modulation of neuronal activity by glial cells in the retina. *J. Neurosci.* 18, 4022–4028. <https://doi.org/10.1523/jneurosci.18-11-04022.1998>.
 49. Li, A., Zhang, X., Zheng, D., Ge, J., Laties, A.M., and Mitchell, C.H. (2011). Sustained elevation of extracellular ATP in aqueous humor from humans with primary chronic angle-closure glaucoma. *Exp. Eye Res.* 93, 528–533. <https://doi.org/10.1016/j.exer.2011.06.020>.
 50. Pérez de Lara, M.J., Guzmán-Aránguez, A., de la Villa, P., Díaz-Hernández, J.I., Miras-Portugal, M.T., and Pintor, J. (2015). Increased levels of extracellular ATP in glaucomatous retinas: possible role of the vesicular nucleotide transporter during the development of the pathology. *Mol. Vis.* 21, 1060–1070.
 51. Newman, E.A. (2001). Propagation of intercellular calcium waves in retinal astrocytes and Müller cells. *J. Neurosci.* 21, 2215–2223. <https://doi.org/10.1523/jneurosci.21-07-02215.2001>.
 52. Ji, M., Miao, Y., Dong, L.D., Chen, J., Mo, X.F., Jiang, S.X., Sun, X.H., Yang, X.L., and Wang, Z. (2012). Group I mGluR-mediated inhibition of Kir channels contributes to retinal Müller cell gliosis in a rat chronic ocular hypertension model. *J. Neurosci.* 32, 12744–12755. <https://doi.org/10.1523/jneurosci.1291-12.2012>.
 53. Li, X., Lv, J., Li, J., and Ren, X. (2021). Kir4.1 may represent a novel therapeutic target for diabetic retinopathy (Review). *Exp. Ther. Med.* 22, 1021. <https://doi.org/10.3892/etm.2021.10453>.
 54. Junaid, A., Moon, M.C., Harding, G.E.J., and Zahradka, P. (2007). Osteopontin localizes to the nucleus of 293 cells and associates with polo-like kinase-1. *Am. J. Physiol. Cell Physiol.* 292, C919–C926. <https://doi.org/10.1152/ajpcell.00477.2006>.
 55. Cantor, H., and Shinohara, M.L. (2009). Regulation of T-helper-cell lineage development by osteopontin: the inside

- story. *Nat. Rev. Immunol.* 9, 137–141. <https://doi.org/10.1038/nri2460>.
56. Yu, H., Liu, X., and Zhong, Y. (2017). The effect of osteopontin on microglia. *BioMed Res. Int.* 2017, 1879437. <https://doi.org/10.1155/2017/1879437>.
57. Ashkar, S., Weber, G.F., Panoutsakopoulou, V., Sanchirico, M.E., Jansson, M., Zawadeh, S., Rittling, S.R., Denhardt, D.T., Glimcher, M.J., and Cantor, H. (2000). Eta-1 (osteopontin): an early component of type-1 (cell-mediated) immunity. *Science* 287, 860–864. <https://doi.org/10.1126/science.287.5454.860>.
58. Shinohara, M.L., Jansson, M., Hwang, E.S., Werneck, M.B.F., Glimcher, L.H., and Cantor, H. (2005). T-bet-dependent expression of osteopontin contributes to T cell polarization. *Proc. Natl. Acad. Sci. USA* 102, 17101–17106. <https://doi.org/10.1073/pnas.0508666102>.
59. Yokosaki, Y., Matsuura, N., Sasaki, T., Murakami, I., Schneider, H., Higashiyama, S., Saitoh, Y., Yamakido, M., Taooka, Y., and Sheppard, D. (1999). The integrin alpha(9) beta(1) binds to a novel recognition sequence (SVVYGLR) in the thrombin-cleaved amino-terminal fragment of osteopontin. *J. Biol. Chem.* 274, 36328–36334. <https://doi.org/10.1074/jbc.274.51.36328>.
60. Smith, L.L., Cheung, H.K., Ling, L.E., Chen, J., Sheppard, D., Pytela, R., and Giachelli, C.M. (1996). Osteopontin N-terminal domain contains a cryptic adhesive sequence recognized by alpha9beta1 integrin. *J. Biol. Chem.* 271, 28485–28491.
61. Scatena, M., Liaw, L., and Giachelli, C.M. (2007). Osteopontin: a multifunctional molecule regulating chronic inflammation and vascular disease. *Arterioscler. Thromb. Vasc. Biol.* 27, 2302–2309. <https://doi.org/10.1161/atvbaha.107.144824>.
62. Gao, Y.L., Xing, L.Q., Ren, T.J., Hou, J.F., Xue, Q., Liu, C., and Han, Y.M. (2016). The expression of osteopontin in breast cancer tissue and its relationship with p21ras and CD44V6 expression. *Eur. J. Gynaecol. Oncol.* 37, 41–47.
63. Yang, L., Shang, X., Zhao, X., Lin, Y., and Liu, J. (2012). [Correlation study between OPN, CD44v6, MMP-9 and distant metastasis in laryngeal squamous cell carcinoma]. *Lin Chung Er Bi Yan Hou Tou Jing Wai Ke Za Zhi* 26, 989–992.
64. Kim, J.S., Bashir, M.M., and Werth, V.P. (2012). Gottron's papules exhibit dermal accumulation of CD44 variant 7 (CD44v7) and its binding partner osteopontin: a unique molecular signature. *J. Invest. Dermatol.* 132, 1825–1832. <https://doi.org/10.1038/jid.2012.54>.
65. Esposito, E., Hayakawa, K., Ahn, B.J., Chan, S.J., Xing, C., Liang, A.C., Kim, K.W., Arai, K., and Lo, E.H. (2018). Effects of ischemic post-conditioning on neuronal VEGF regulation and microglial polarization in a rat model of focal cerebral ischemia. *J. Neurochem.* 146, 160–172.
66. Liu, X., Huang, P., Wang, J., Yang, Z., Huang, S., Luo, X., Qi, J., Shen, X., and Zhong, Y. (2016). The effect of A2A receptor antagonist on microglial activation in experimental glaucoma. *Invest. Ophthalmol. Vis. Sci.* 57, 776–786.
67. Hicks, D., and Courtois, Y. (1990). The growth and behaviour of rat retinal Müller cells in vitro. 1. An improved method for isolation and culture. *Exp. Eye Res.* 51, 119–129. [https://doi.org/10.1016/0014-4835\(90\)90063-z](https://doi.org/10.1016/0014-4835(90)90063-z).
68. Tan, H.B., Shen, X., Cheng, Y., Jiao, Q., Yang, Z.J., and Zhong, Y.S. (2012). Evaluation of a partial optic nerve crush model in rats. *Exp. Ther. Med.* 4, 401–404. <https://doi.org/10.3892/etm.2012.619>.
69. Zayas-Santiago, A., Ríos, D.S., Zueva, L.V., and Inyushin, M.Y. (2018). Localization of α -crystallin in rat retinal müller glial cells and photoreceptors. *Microsc. Microanal.* 24, 545–552. <https://doi.org/10.1017/s1431927618015118>.
70. Pfaffl, M.W. (2001). A new mathematical model for relative quantification in real-time RT-PCR. *Nucleic Acids Res.* 29, e45.

STAR★METHODS

KEY RESOURCES TABLE

REAGENT or RESOURCE	SOURCE	IDENTIFIER
Antibodies		
Anti-GAPDH antibody	Abcam	Cat#ab128797
Anti-CD68 antibody	Abcam	Cat#ab125212
Anti-Iba-1 antibody	Abcam	Cat#ab178846
Anti-OPN antibody	Abcam	Cat#ab8448
Anti-CD44 antibody	Abcam	Cat#ab157107
Anti-Itgαvβ3 antibody	Abcam	Cat#ab179475
Anti-P62 antibody	Cell Signaling Technology	Cat#23214
Anti-LC3B antibody	Cell Signaling Technology	Cat#12741
Anti-Atg5 antibody	Abcam	Cat#ab108327
Anti-Atg12 antibody	Abcam	Cat#ab303488
Anti-Beclin1 antibody	Cell Signaling Technology	Cat#3495
Alexa Fluor@555 Donkey Anti-Rabbit IgG	Invitrogen	Cat#A31572
Alexa Fluor@488 Donkey Anti-Mouse IgG	Invitrogen	Cat#A32766
SB203580	Selleck	Cat#S1076
Cyclo(RGDyK)	Selleck	Cat#7844
minocycline	Sigma-Aldrich	Cat#M9511
Bacterial and virus strains		
Ad-CMV-RFP-GFP-LC3	Bioengine	N/A
Chemicals, peptides, and recombinant proteins		
HyStem Cell Culture Scaffold Kit	Sigma-Aldrich	Cat#HYSC010
DMEM	Gibco	Cat#11960-044
Fetal bovine serum	Gibco	Cat#10100-147
PrimeScript™ RT Master Mix (Perfect Real Time)	TakaRa	Cat#RR036A
TB Green™ Premix Ex Taq™	TakaRa	Cat#RR071A
Matrigel® Basement Membrane Matrix	Corning	Cat#356237
DAPI	Beyotime	Cat#C1002
Fluoro gold	Fluorochrome	Cat#52-9400
Critical commercial assays		
BCA Protein Assay kit	Beyotime	Cat# P0012S
Lipofectamine 3000	Invitrogen	Cat# L3000015
Experimental models: Organisms/strains		
Sprague-Dawley (SD) male grown-up rodents	Zhejiang Vital River Laboratory Animal Technology Co., Ltd (Zhejiang, China)	SCXK (Zhe) 2019-0001
Oligonucleotides		
primer sequences for PCR	This Paper	N/A
siRNA targeting sequence	This Paper	N/A
Recombinant DNA		
SiR-OPN	Life Technologies	N/A
oe-OPN	Bioengine	N/A

(Continued on next page)

Continued

REAGENT or RESOURCE	SOURCE	IDENTIFIER
Software and algorithms		
GraphPad Prism 8.0	GraphPad	https://www.graphpad.com/
ImageJ	NIH, USA	https://imagej.nih.gov/ij

RESOURCE AVAILABILITY

Lead contact

Further information and requests for resources and reagents should be directed to and will be fulfilled by the lead contact Yisheng Zhong (yszhong68@126.com).

Materials availability

This study did not generate new unique reagents.

Data and code availability

- All data reported in this paper will be shared by the [lead contact](#) upon reasonable request.
- This paper does not report original code.
- Any additional information required to reanalyze the data reported in this paper is available from the [lead contact](#) upon request.

EXPERIMENTAL MODEL AND SUBJECT DETAILS

Animals

The experiment was endorsed by Ruijin Hospital, Shanghai, China. All tasks followed the Association for Research in Vision and Ophthalmology (ARVO) rules. Sprague-Dawley (SD) male grown-up rodents, weighing roughly 250 g, were sourced from Zhejiang Vital River Laboratory Animal Technology Co., Ltd (Zhejiang, China) and taken care of under a 12 hour light and dim cycle.

Primary rat retinal microglia cultures

Microglial cells were isolated from the retinas of newborn rats within 48 hours after birth as described previously with minor modifications.^{65,66} In brief, retinas were washed using ice-cold PBS, then digested for 1 minute at 37°C using 0.125% trypsin-EDTA (Invitrogen, Carlsbad, CA) that contains DNase I (100 U/mL; Sigma-Aldrich). Cells were collected after centrifugation and resuspended by introducing Dulbecco's modified Eagle's medium (DMEM; Gibco, NY) that contains 4.5 g/L glucose supplemented with 20% fetal bovine serum (FBS). Cells were then plated in 75 cm² culture flasks at a density of approximately 13 × 10⁷/ml, and cultured under 5% CO₂ at 37°C in a humidified incubator. Culture medium was replaced 48 hours after plating, and the semi-replacement of the culture medium was performed once every week thereafter. Two weeks later, microglial cells were isolated from the cultured total glial cells by shaking the culture flasks at 90-120 rpm for 90 minutes and resuspended in culture medium. The cells were identified using immunocytochemical staining of CD11b and Iba-1.

Primary rat Müller cells cultures

Primary Müller cells were isolated and cultured as described previously with minor modifications.⁶⁷ In brief, eyeballs were enucleated from newborn rats within 48 hours after birth and the retinas were detached after soaking the globes in a growth medium overnight. The retinas were digested with enzymes for 2 hours, dissociated in a stationary culture and maintained in another stationary culture of 10% serum supplemented growth medium. Cultures displayed extensive cellular outgrowth after 3–5 days, with abundant fusiform and epithelioid cells. Removal of aggregates and cellular debris after 6–7 days brought off isolation of primary Müller cells. The cells were identified by immunocytochemical staining of glutamine synthetase (GS) and glial fibrillary acidic protein (GFAP).

METHOD DETAILS

Anesthesia of rats

Prior to medical procedure, xylazine (10 mg/kg; Sigma–Aldrich, St. Louis, MO) and ketamine hydrochloride (25 mg/kg; Sigma–Aldrich) were utilized for foundational sedation of the rodents through intraperitoneal infusion. For the eyes being worked, a drop of 0.5% proparacaine hydrochloride (Bausch and Lomb, Tampa, FL) was utilized for effective sedation.

Prior to IOP estimations, rodents were anesthetized utilizing isoflurane inward breath (2–4%; Sigma–Aldrich).

Induction of IOP elevation

The chronic ocular hypertension (COH) was induced by infusing HyStem Cell Culture Scaffold kit (HCCS; Sigma–Aldrich) into the front chamber, which comprises of HyStem (a thiol-altered carboxymethyl hyaluronic corrosive) and Extralink (a thiol-receptive polyethylene glycol diacrylate). HyStem and Extralink were first disintegrated in degassed water and blended at a proportion of 4:1 preceding the infusion. 7 μ L new fluid combination was then infused gradually into the front office of the correct eye more than 1 minute with a 31-gauge insulin syringe (BD Ultra-Fine, Franklin Lakes, NJ). The blend was set for 5 minutes to take into consideration cross-connecting gelation *in situ*. To keep fluid combination from spilling over before gelation, the needle was left in the front chamber all through this cycle. An equal amount of phosphate buffer saline (PBS) was injected into the right eyes of control group rats. 0.3% Ofloxacin Eye Ointment (Santen Pharmaceutical, Osaka, Japan) was used to prevent infections.

IOP measurement

Measurement of IOP was completed using a TonoLab Rebound Tonometer (Icare, Vantaa, Finland). Measurements were taken before COH to acquire a baseline, and every 2nd day after intracameral injection. All measurements were conducted between 10 AM and 2 PM to eliminate bias. Averages of 6 readings for each measurement were recorded and the data are presented as point-plot graphs (Figures 1A, 2F, 3A, and 5D).

Intravitreal injection

The pupil of the anesthetized eye was dilated with tropicamide drops. A 32-gauge needle was inserted 2 mm behind the temporal limbus and directed toward the optic nerve to make an access for drug delivery. Subsequently, one dose of 2 μ L OPN (500ng/ml, diluted in PBS; Merck KGaA, Darmstadt, Germany), OPN neutralizing antibody (Anti-OPN, 50 μ M, diluted in PBS; Merck KGaA), CD44 neutralizing antibody (Anti-CD44, 20 μ g/ml, diluted in PBS, R&D systems China Co. Ltd), Selective inhibitor of Itg α V β 3 (cyclo RGDyk, 20nM, diluted in 0.2% DMSO, Selleckchem, Houston, TX, USA), minocycline (50 μ M, diluted in PBS, Sigma-Aldrich, St. Louis, MO, USA) or SB203580 (50 μ M, diluted in 0.2% DMSO; Sigma Aldrich) was injected into the vitreous cavity through the access using a microinjector (Hamilton Bonaduz AG, Switzerland) under a stereoscopic microscope (Carl Zeiss Microscopy, Jena, Germany) according to experimental needs. Each eye that received only an injection of PBS or 0.2% DMSO in the same manner served as a negative control.

Retrograde labeling and quantification of RGCs

One week before sacrificing rats, the retrograde labeling of RGCs by injections of Fluoro-Gold (4%, dissolved in 0.9% saline; Fluorochrome, Denver, CO) into the bilateral superior colliculi was performed as previously described.⁶⁸ Briefly, following the removal of skin and muscles, the cranium pierce location was set at the bilateral points 6.4 mm behind the fonticuli anterior, 1.5 mm apart from the midline and then inserting the needle 4.0 mm deep from the skull surface. 4 μ L of Fluoro-Gold solution was injected at each point by micro injector. Seven days after the labeling, the retinal neuroepithelium layers were dissociated and wholly mounted on slides. All operations were protected from light. Images of labeled RGCs were captured by a Zeiss Imager M1 laser-scanning microscope (Carl Zeiss Microscopy, Jena, Germany). The quantification of RGCs was conducted in areas of approximately the same distances of 1/6, 3/6, 5/6 retinal radius from the optic disk in each quadrant, using a digital image-analysis system (Image Pro Plus Version 6.0; Media Cybernetics, Silver Spring, MD). The average of three RGC densities at the same eccentricity was considered as the mean density of RGCs for the certain position in each retina.

Cell treatments with OPN

Müller cells of passage 2 were resuspended and seeded in 10cm cell culture dish and 24-well plates with or without cover-slips. One 24h after seeding, the cells were incubated in the medium containing 6.25 µg/mL OPN for 0, 12, 24, and 48 hours. Cells in 10cm cell culture dish were used for transmission electron microscope, while cells in 24-well plates were collected for Western blot and qRT-PCR, cells on cover glasses were used for immunocytochemistry analysis.

Transfection of siRNA

OPN expression was silenced using an OPN-specific siRNA (small interfering RNA, Life Technologies, Grand Island, NY). Cells were seeded in 24-cell plates with medium containing 20% FBS 24 hours before transfection, reaching approximately 80% confluency. siRNA (50nM, target sequence: GGCUUACGGA CUGAGGUCAAA) was complexed with Lipofectamine 3000 (Invitrogen) according to the manufacturer's instructions and applied to each control plate. The cells were classified into four groups: blank group, liposome group, non-targeting siRNA group and targeting siRNA group. After 24 hours, cells were collected and RNA was extracted for analysis.

Plasmids transfection and transient expression of OPN

Lipofectamine 3000 (Invitrogen) was used to transfect the plasmids into primary microglia. Full-length complementary cDNAs of OPN were synthesized and inserted into the expression vector pcDNA3.1 (Bioengine, Shanghai, China). The plasmids were subjected to DNA sequencing for verification.

Preparation of three-dimensional matrigel matrix

The preparation of a three-dimensional matrigel matrix (Corning, Corning, NY) was done following the manufacturer's instructions. An ice bath was used to precool the matrigel matrix and materials that would come in contact with the cells. The matrigel matrix was then diluted with DMEM containing 4.5 g/L glucose at a ratio of 1:1. Primary microglia cells were then suspended slowly in the diluted matrix using a pipette at a density of 3×10^6 /mL. The matrix containing cells was then placed in six-well BioPress™ compression culture plates (Flexcell International Corporation, Burlington, NC). The plates were then transferred to an incubator with 5% CO₂ at 37°C., where the matrix solution transformed into gel after 30 minutes. A serum-free medium was then added gently around the matrigel. Cells were seeded overnight in the incubator.

Pressure loading of cell cultures

Pressure loading to the cells was accomplished with the Flexcell® FX-5000™ Compression System (Flexcell International Corporation). Microglia cells in six-well BioPress™ compression culture plates were placed in a specially designed half-closed container. The pressure of the compression system was set at 5kPa with a frequency of 0.1 Hz. The endurance was set at 2, 4, 6, and 8h under computerized control. Once pressuring concludes, the cells were immediately collected from the matrigel matrix for RNA or protein extraction. For OPN overexpression or suppression, the microglial cells were pretreated with oe-OPN (10 nM) or SiR-OPN (50 nM) 12 hours before compression loading. For suppression of microglial activation, the microglial cells were pretreated with minocycline (50 µM) 12 hours before compression loading.

Transfection of Ad-CMV-RFP-GFP-LC3 and evaluation of fluorescent LC3 puncta

The Ad-CMV-RFP-GFP-LC3 was purchased from Shanghai Bioengine Co., Ltd. The Müller cells were transfected with 15 M.O.I. (multiplicity of infection) of Ad-CMV-RFP-GFP-LC3 adenovirus for 24h and then treated with OPN or corresponding condition medium. The cells were washed with PBS, fixed with 4% paraformaldehyde, and viewed under a confocal fluorescence microscope (Nikon, A1, Tokyo, Japan). GFP degrades in an acidic environment while RFP does not. Thus, yellow dots (formed out of the overlap between red and green) indicate autophagosomes, while red dots indicate autophagic lysosomes. The number of GFP and mRFP dots was determined by manual counting of fluorescent puncta in six fields.

Transmission electron microscope

The cells or retinal tissues (2 × 2 × 2 mm) were fixed with 2.5% glutaraldehyde and 1% osmium tetroxide followed by dehydration in an increasing concentration series of ethanol. The samples were embedded in Durcupan ACM (Sigma-Aldrich) for 6 h, and ultrathin sections were cut using a Leica Ultramicrotome EM UC6 (Leica, Wetzlar, Germany). The sections were then stained with uranyl acetate and lead citrate, and examined with a Tecnai G2 12 transmission electron microscope (Thermo Fisher Scientific, Hillsboro,

Oregon USA). Skilled electron microscopy technicians handled observation of Müller cells autophagolysosome counting. Images were then collected and analyzed. In short, the cytoplasm of Müller cells is more osmiophilic than the cytoplasm of near cells and looks darker. Please refer to previous literature for specific methods.⁶⁹

Immunofluorescence

For the preparation of retinal tissue sections, the ocular anterior segments were removed to preserve the eyecups, which were frozen in an Optimum Cutting Temperature compound (OCT; Sakura Finetek, Torrance, CA), and then 10- μ m-thick cryosections were cut and air-dried. The retinal sections or cells on coverslips were permeated with cold 0.25% Triton X-100 solution (Sigma-Aldrich) for 30 minutes, then blocked in 1% BSA at room temperature for 1 hour. The slices were incubated with anti-GS (1:100 dilution; Abcam, Cambridge, England, ab64613), anti-CD44 (1:1000 dilution; Abcam, ab157107), anti-Itg α v β 3 (1:500 dilution; Abcam, ab179475), anti-LC-3B (1:100 dilution; Cell Signaling Technology, Massachusetts, USA, 12741) or anti-P62 (1:800 dilution; Cell Signaling Technology, 23214) primary antibodies at 4°C overnight under single or combined application as needed. Then, they were incubated with Texas-red conjugated donkey anti-rabbit (1:1000 dilution; Abcam) and FITC conjugated donkey anti-mouse (1:1000 dilution; Abcam) secondary antibodies at room temperature for 1 hour. The samples were further incubated with 4',6-diamidino-2-phenylindole (DAPI; Sigma-Aldrich) for 5 minutes and examined under microscopy (Carl Zeiss Microscopy).

Western blot analysis

Total protein was extracted from rat retina or Müller cells using RIPA lysis buffer (Sigma-Aldrich) with a cocktail of protease inhibitors (Roche Applied Science, Penzberg, Germany) following the manufacturer's instructions. The protein expression level was determined by densitometric analysis and normalized to the level of GAPDH. Since different proteins with similar molecular weights were sourced from different gels and PVDF membranes, a separate GAPDH control was run for each blot and one of them was chosen for presentation. The primary antibodies were as follows: GAPDH (1:10000 dilution; Abcam, ab8245), CD11b (1:1000 dilution; Abcam, ab128797), CD68 (1:1000 dilution; Abcam, ab125212), Iba-1 (1:1000 dilution; Abcam, ab178846), OPN (1:1000 dilution; Abcam, ab8448), CD44 (1:5000 dilution; Abcam, ab157107), Itg α v β 3 (1:5000 dilution; Abcam, ab179475), P62 (1:1000 dilution; Cell Signaling Technology, 23214), LC3B (1:1000 dilution; Cell Signaling Technology, 12741), Atg5 (1:5000 dilution; Abcam, ab108327), Atg12 (1:1000 dilution; Abcam, ab303488), Beclin1 (1:1000 dilution; Cell Signaling Technology, 3495).

Quantitative real-time RT-PCR

Total RNA was isolated from rat retina or Müller cells using Trizol reagent (Invitrogen) following the manufacturer's instructions. The RNA was then converted to cDNA using the reverse transcriptase kit PrimeScript RT Master Mix (Takara Bio, Inc., Shiga, Japan). Primers were designed using Primer Premier 5.0 software (Thermo Fisher Scientific, Grand Island, NY). The primer pairs used were as follows:

β -actin (F: CACTATCGGCAATGAGCGGTTCC, R: CAGCACTGTGTTGGCATAGAGGTC),

OPN (F: ACGACGATGACGACGGAGACC, R: GTGTGCTGGCAGTGAAGGACTC),

Iba-1 (F: AACGTCTCCTCGGAGCCACTG, R: GCTGGAGAACTTGGGGTTCCC),

CD11b (F: GGGCAGGAGACGTTTGTGAAGG, R: GCCAGCAGTGATGAGAGCCAAG),

CD68 (F: GTCTGACCTTGCTGGTACTGCTTG, R: CGTAGGGCTTGCTGTGCTTCC)

CD44 (F: CCTGGCACAGCAGCAGATCG, R: TGGGCAAGGTGGTGTGAAAGC)

Itg α v (F: TGCTGCTCGGCCTCCTACTG, R: CGAAGAAGTCCACGGCGAATCC)

Itg β 3 (F: GACTCGGACTGGACTGGCTACTAC, R: ACTTCTCGCAGGTGTCTCCATAGG)

P62 (F: TCGTGGTCGTGGGGTGTCTG, R: TCTGGTGATGGAGCCTTACTGG)

Atg5 (F: CTCAGCTCTGCCTTGGAAACATCAC, R: AAGTGAGCCTCAACTGCATCCTTG)

Atg12 (F: TCTCCCCAGAAACAGCCATCCC, R: AGTGTCTCTACAGCCTTCAGCAG)

Beclin1 (F: TCAAGATCCTGGACCGAGTGACC, R: TCCTGGCTCTCTCCTGGTTTCG)

LC3B (F: AGCCTTCTTCCTCCTGGTGAATGG, R: AGTGCTGTCCCGAACGTCTCC).

Quantitative real-time PCR was performed using the SYBR Premix Ex Taq II kit (Takara Bio, Inc.) in a total volume of 20 μ L on a 7500 real-time PCR (Applied Biosystems, Foster City, CA) employing a procedure of 95°C for 30 seconds, 40 cycles of 95°C for 5 seconds, 60°C for 34 seconds, and 72°C for 30 seconds. mRNA contents of each sample were detected in duplicates. β -Actin was used as a reference gene. Relative quantification of each gene expression was calculated using the $2^{-\Delta\Delta C_t}$ method as described previously.⁷⁰

QUANTIFICATION AND STATISTICAL ANALYSIS

Statistical analyses were performed with GraphPad Prism 8.0. Statistical differences between groups were estimated using a Student's t-test or one-way analysis of variance (ANOVA). The data were expressed as the mean \pm SD of at least three measurements. Statistical significance was designated for analyses with $p < 0.05$. The numbers of samples (n) are plotted explicitly in each graph. Asterisks in all figures indicate the degree of significant differences compared to controls (* $P < 0.05$, ** $P < 0.01$, *** $P < 0.001$, **** $P < 0.0001$).